Constant Velocity Types

Double Cardan Universal Joint

Double Cardan Universal Joint—A near constant velocity universal joint which consists of two Cardan universal joints whose crosses are connected by a coupling yoke with internal supporting and centering means and has intersecting shaft axes. At the design joint angle and at zero, the instantaneous angular velocity ratio is unity, while at other joint angles it is near unity.

Coupling Yoke—A double yoke which connects the two halves of a double Cardan universal joint.

Socket Yoke—A yoke incorporating a socket.

Socket—A separate bearing member or integral cavity in a yoke used to pivotally locate and support the ball of a ball and socket type centering device.

Ball and Socket Type Centering Device—A mechanism which functions as a self-aligning bearing and provides internal supporting and centering means for a double Cardan type universal joint. The two basic types of ball and socket designs are the centering ball and stud and the ball stud and seat constructions.

Centering Stud Yoke—A yoke incorporating a centering stud.

Centering Stud—A part of a yoke used to support a centering ball.

Centering Ball—A partly spherical-shaped member which pivots and provides supporting and centering means.

Ball Stud Yoke—A yoke incorporating a ball stud.

Ball Stud—A partly spherical-shaped part of a yoke which pivots and provides supporting and centering means.

Ball Seat—A full or segmented ring-like angular contact bearing member located in a socket which supports and centers the ball stud.

Double Cardan Universal Joint (Trunnion Pin Type)

Double Cardan Universal Joint (Trunnion Pin Type)—A near constant velocity universal joint which consists of two trunnion pin type Cardan universal joints whose trunnion yokes are connected by a coupling yoke with internal supporting and centering means, and has intersecting shaft axes. At the design joint angle and at zero, the instantaneous angular velocity ratio is unity, while at other joint angles it is near unity.

Coupling Yoke—A double yoke which connects the two halves of a trunnion pin type double Cardan universal joint.

Trunnion Yoke—A yoke which has a pair of opposing trunnions.

Trunnion Pin—A member pressed transversely through the shaft which provides trunnions for the universal joint bearings.

Double Cardan Universal Joint (Twin Ball and Centering Plate Type)

Double Cardan Universal Joint (Twin Ball and Centering Plate Type)—A constant velocity universal joint which consists of two Cardan universal joints whose crosses are connected by a two piece flanged coupling yoke with internal supporting and centering means and has intersecting shaft axes. At all operating angles within the design range, the instantaneous angular velocity ratio is unity.

Coupling Yoke—A double yoke consisting of two flange type yokes which supports the socket and centering plate and connects the two halves of a twin ball and centering plate type double Cardan universal joint.

Socket and Centering Plate—A disc type member which supports and centers the ball studs.

Wear Plate—A circular plate type member which provides a bearing surface for the socket and centering plate.

Tracta Universal Joint

Tracta Universal Joint—A near constant velocity universal joint which consists of two yokes drivably connected through plane bearing surfaces to two intermediate couplings similarly engaged, and requires external supporting, centering, and sealing means.

Fork Yoke—A fork-shaped member with plane surfaces used for engaging the mating groove of an intermediate coupling and with drivable means of attachment.

Tongue and Groove Coupling—A hemispherically-shaped intermediate member with tongue and groove located normal to each other.

Grooved Coupling—A hemispherically-shaped intermediate member with two grooves located normal to each other.

Tripot Universal Joint (End Motion Type)

Tripot Universal Joint (End Motion Type)—A constant velocity universal joint, radially self-supported and permitting axial movement, which consists of a housing drivably connected to a shaft through three equally spaced trunnion mounted balls.

Housing—A member with three equally spaced partly cylindrical axial ball bores on the cylindrical inner clearance surface and with drivable means of attachment. In the tulip type housing, these ball bores have open circular segments on the periphery, as well as on the inner clearance surface.

Spider—A member with three equally spaced trunnions in the same plane and with internally splined drivable means of attachment.

Ball—A partly spherical-shaped member which pivots and transmits torque from the housing to the shaft through the spider and permits axial movement. Generally, needle rollers are used between the ball and the spider.

Thrust Washer—A member which radially positions the needle rollers on the spider trunnion.

Housing Cover—A sleeve-like member which encloses the tulip type housing and provides for attachment of the boot seal.

Band—A ring-like metallic or nonmetallic member used to hold the boot seal in position on the universal joint.

Retaining Ring—A removable member used as a shoulder for retaining and positioning universal joint components in an assembly.

Tripot Universal Joint (Fixed Center Type)

Tripot Universal Joint (Fixed Center Type)—A self-supported constant velocity universal joint which consists of a housing drivably connected to a forked shaft through three

American Axle v. Neapco - IPR2025-00090
PET_AAM_1012-0339

equally spaced trunnion mounted balls and retained as an assembly by a retaining clip. The joint center is maintained in a substantially fixed axial location by means of a spring loaded centering device.

Housing—A bell-shaped member retaining a spider with rotating and sliding balls mounted on three equally spaced trunnions located in the same plane, and with drivable means of attachment.

Ball—A partly spherical-shaped member which pivots and transmits torque from the housing to the shaft through the spider.

Forked Shaft—A member with tulip-shaped prongs incorporating three equally spaced partly cylindrical axial ball bores, and with drivable means of attachment.

Retaining Clip—A three pronged spider-like member which retains the universal joint as an assembly.

Centering Button—A thrust loaded member which locates the universal joint center.

Rzeppa Universal Joint

Rzeppa Universal Joint—A self-supported constant velocity universal joint which consists of an outer and inner race drivably connected through balls positioned in the constant velocity plane by axially offset meridionally curved grooves and maintained in this plane by a cage located between the two races.

Outer Race (Bell Type)—A bell-shaped member with axially offset meridionally curved ball grooves on the partly spherical inner bearing surface and with drivable means of attachment.

Outer Race (Disc Type)—An annular member with axially offset meridionally curved ball grooves on the partly spherical inner bearing surface and with drivable means of attachment.

Inner Race—An annular member with axially offset meridionally curved ball grooves on the partly spherical outer bearing surface and with internally splined drivable means of attachment.

Cage—A ring-like member with concentric outer and inner partly spherical bearing surfaces and with a circumferential series of openings or windows for maintaining balls in a common plane.

Ball—One of the intermediate drive members of a ball type constant velocity universal joint.

Ball Spline Rzeppa Universal Joint

Ball Spline Rzeppa Universal Joint—A disc type Rzeppa universal joint which permits axial movement by means of an integral ball spline.

Outer Housing—An annular member with axial ball spline grooves on the cylindrical inner surface and with drivable means of attachment.

Inner Housing—A disc type Rzeppa outer race with axial ball spline grooves on its cylindrical outer surface.

Weiss Universal Joint (End Motion Type)

Weiss Universal Joint (End Motion Type)—A constant velocity universal joint, radially self-supported and permitting axial movement, which consists of two yokes drivably connected through balls positioned and maintained in the constant velocity plane by inclined intersecting straight grooves, located in radial planes or by parallel pairs of inclined intersecting straight grooves symmetrically located about radial planes.

Ball Yoke—A yoke-shaped member with inclined straight ball grooves located in radial planes or by parallel pairs of inclined straight ball grooves symmetrically located about radial planes on the side of the yoke ears and with drivable means of attachment.

Seal Retainer—A member used to hold the boot seal in position on the ball yoke.

Weiss Universal Joint (Fixed Center Type)

Weiss Universal Joint (Fixed Center Type)—A constant velocity universal joint, radially self-supported, which consists of two yokes drivably connected through balls positioned and maintained in the constant velocity plane by axially offset intersecting curved grooves, located in radial planes and retained as an assembly by a centering ball. An external seal and axial support means are required.

Ball Yoke—A yoke-shaped member with curved ball grooves located in radial planes on the side of the yoke ears and with drivable means of attachment.

Centering Ball—A ball which centers the universal joint, absorbs end thrust, and has a hole for a pin that positions the universal joint components as an assembly.

Centering Ball Pin—A pin which positions the centering ball.

Retaining Pin—A pin which positions the centering ball pin in the pilot hole of the centering ball.

Cross Groove Universal Joint

Cross Groove Universal Joint—A constant velocity universal joint, radially self-supported, which consists of an outer and inner race drivably connected through balls located in circumferentially spaced straight or helical grooves, alternately inclined relative to the rotational axis. The balls are positioned in the constant velocity plane by an intersecting groove relationship and maintained in this plane by a cage located between the two races. The joint permits axial movement since the cage is not positionably engaged to either race.

Outer Race—A member with circumferentially spaced straight or helical ball grooves alternately inclined on the cylindrical inner surface and with drivable means of attachment.

Inner Race—An annular member with circumferentially spaced straight or helical ball grooves alternately inclined on the partly spherical or conical outer surfaces and with internally splined drivable means of attachment.

Cage—A ring-like member with concentric outer and inner cylindrical or partly spherical or conical surfaces, and with a circumferential series of openings or windows for maintaining balls in a common plane.

Seal Adapter—A member used to connect the boot seal to the outer race.

Outer Race End Cover—A member which protects the universal joint from contamination and loss of lubricant during shipping and handling.

Double Offset Universal Joint (End Motion Type)

Double Offset Universal Joint (End Motion Type)—A constant velocity universal joint, radially self-supported, which consists of an outer and inner race drivably connected through balls located in axially straight grooves. The balls are positioned and

American Axle v. Neapco - IPR2025-00090
PET_AAM_1012-0340

maintained in the constant velocity plane by a cage with axially offset spherical surfaces located between the two races. The joint permits axial movement since the cage is positionably engaged only by the inner race.

Outer Race—A member with axially straight ball grooves on the cylindrical inner bearing surface and with drivable means of attachment.

Inner Race—An annular member with axially straight ball grooves on the partly spherical outer bearing surface and with internally splined drivable means of attachment.

Cage—A ring-like member with axially offset outer and inner partly spherical bearing surfaces, and with a circumferential series of openings or windows for maintaining balls in a common plane.

Seal Retainer—A member used to hold the boot seal in position on the outer race.

Double Offset Universal Joint (Fixed Center Type)

Double Offset Universal Joint (Fixed Center Type)—A self-supported constant velocity universal joint which consists of an outer and inner race drivably connected through balls located in axially straight grooves. The balls are positioned and maintained in the constant velocity plane by a cage with axially offset spherical surfaces located between the two races.

Outer Race—An annular member with axially straight ball grooves on the partly spherical inner bearing surface and with drivable means of attachment.

American Axle v. Neapco - IPR2025-00090
PET_AAM_1012-0341

Appendices

American Axle v. Neapco - IPR2025-00090
PET_AAM_1012-0343

APPENDIX A

Hertz Contact Stress, Stress and Strength Gradients Along the Load Axis, Allowable Compressive Stress and Determination of Carburized Case Depth

E. R. Wagner, P.E. — Saginaw Steering Gear Div., GMC

NOMENCLATURE

- a, b = Semi-axes of contact area, also used to denote contacting bodies
- E_a, E_b = Moduli of elasticity
- g = Used in contact area computations
- $K(\ ), E(\ )$ = Elliptic integrals
- k, k' = Factors depending on conformity
- L = Length of rectangular contact area
- P_o = Normal load
- S_m = Mean surface compressive stress
- $\sigma_{z\ (max)}$ = Maximum surface compressive stress
- S_s = Maximum subsurface shear stress (at depth Z_1)
- $\sigma_x, \sigma_y, \sigma_z$ = Principal stresses in designated direction
- $\tau_{xy}, \tau_{xz}, \tau_{yz}$ = Maximum shear stresses in designated planes (at 45 deg)
- z = Any depth to elementary particle
- Z_1 = Depth to point of maximum subsurface shear stress
- ϵ = Auxiliary angle depending on conformity
- λ_a, λ_b = Elastic constants
- μ, ν = Hertz factors (transcendental functions)
- δ = Poisson's ratio
- γ = Auxiliary angle depending on conformity
- 1, 2 = Used to denote planes at right angles to one another
- r = Any radius from center of contact circle
- $R_{a1}, R_{a2}, R_{b1}, R_{b2}$ = Principal radii of curvature of curved surfaces
- R_a, R_b = Radii of curvature of cylindrical bodies
- X, Y, Z = Principal axes of elementary particle also principal axes of contact surface
- x, y = Any distance from center of contact area
- $\sum$ = Summation or total
- M = Function of elliptic integral
- Λ = Variable depending on body geometry and material
- $\Omega_x, \Omega_x', \Omega_y, \Omega_y'$ = Functions of elliptic integrals
- A, B = Constants depending on body geometry
- ϕ, θ = Dependent variable functions of elliptic integrals
- ξ = Depth ratio
- $\sigma_{xr}, \sigma_{yr}, \sigma_{zr}$ = Residual stresses in designated direction
- $\sigma_x', \sigma_y', \sigma_z'$ = Resultant principal stresses in designated direction
- τ_{yz}' = Highest resultant maximum shear stress in designated plane (for two contacting cylinders with parallel axes)
- R"c" = Rockwell hardness, "c" scale
- $2Z_1$ = Effective case depth
- $3Z_1$ = Total case depth

Solid Elastic Bodies in Contact

When two solid, elastic curved bodies are pressed together under load, a certain amount of flattening occurs at the contact point. Due to this flattening, there is produced an elliptical pressure or contact area over which the total load is distributed. The relations governing the shape and size of the contact area and the distribution of stress over this area were mathematically investigated by Heinrich Hertz and published in Berlin in January, 1881. Hertz's analysis was based on the assumptions of elastic and isotropic material behavior, loading normal to the surface, and a contact area whose dimensions are relatively small in comparison with the radii of curvature and with the dimensions of the bodies. These relations show good agreement with test results except where the dimensions of the projected contact area are large in comparison to the principal radii of curvature of the contacting bodies.

Although Hertz's work was limited to an analysis of the distribution of stress at the contact surface, more recent investigators extended this analysis to include a consideration of the stress states below the surface, within the contact zone, and have substantiated their results by photo-elastic tests. These studies revealed the presence of important shear stresses in addition to the principal stresses beneath the surface.

Let the bodies be denoted by the subscripts a and b , respectively, as shown in Fig. A-1. Also, let the principal radii of curvature at the contact point be R_{a1} and R_{a2} for body "a" and R_{b1} and R_{b2} for body "b". The radii of curvature are measured in two planes, 1 and 2, at right angles to one another as shown in Fig. A-1, the subscripts 1 and 2 referring to the respective planes.

When body "a" and body "b" are pressed together by the normal load P_o, the resulting contact area whose semi-axes are a and b is shown in Fig. A-2.

Hertz gives the dimensions of the contact area in terms of the transcendental functions μ and ν, as:

$$a = \mu g \qquad \text{Eq. A-1}$$

$$b = \nu g \qquad \text{Eq. A-2}$$

where: Eq. A-3

$$g = \sqrt[3]{\frac{3P_o(\lambda_a + \lambda_b)}{8\left(\frac{1}{R_{a1}} + \frac{1}{R_{a2}} + \frac{1}{R_{b1}} + \frac{1}{R_{b2}}\right)}}$$

Λ_a and Λ_b are elastic constants of the two bodies which depend in turn on the respective values of modulus of

American Axle v. Neapco - IPR2025-00090
PET_AAM_1012-0345

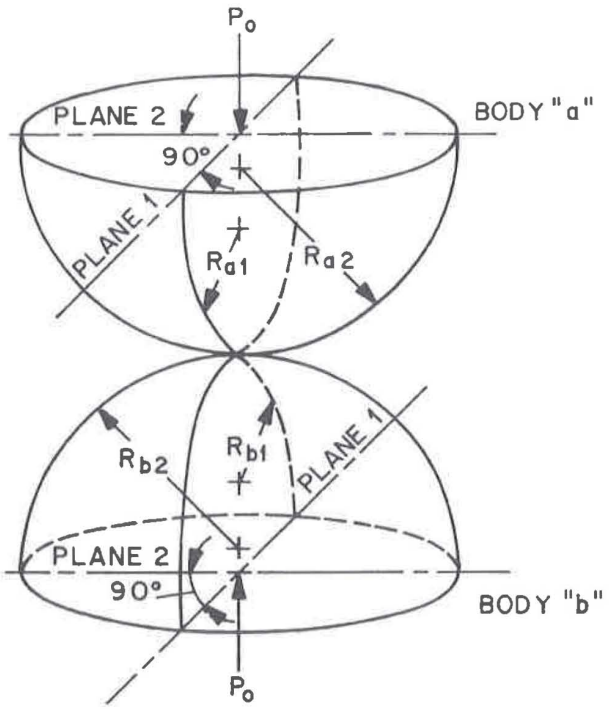


Fig. A-1 — General case of two curved bodies in contact

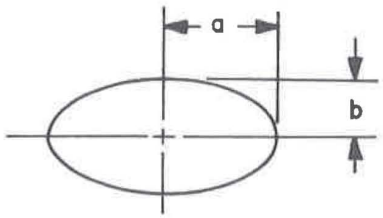


Fig. A-2 — Elliptical contact area

elasticity E and Poisson's ratio δ.

$$\lambda_a = \frac{4(1 - \delta_a^2)}{E_a} \qquad \text{Eq. A-4}$$

$$\lambda_b = \frac{4(1 - \delta_b^2)}{E_b} \qquad \text{Eq. A-5}$$

If both bodies are of steel with a modulus of elasticity 29×10^6 psi and with a Poisson's ratio 0.25, the value of g from Eq. A-3 is:

Eq. A-6

$$g = 0.0045944 \sqrt[3]{\frac{P_o}{\frac{1}{R_{a1}} + \frac{1}{R_{a2}} + \frac{1}{R_{b1}} + \frac{1}{R_{b2}}}}$$

The values of the principal radii of curvature, R_{a1}, R_{a2}, R_{b1} and R_{b2} are taken in accordance with Fig. A-1.

The principal radii of curvature may be either positive or negative, depending on whether the centers of curvature lie within or without the body as shown in Fig. A-3.

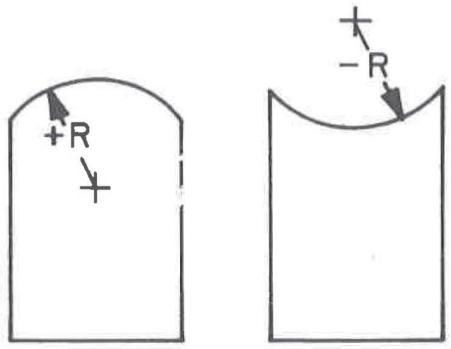


Fig. A-3 — Sign convention for radii of curvature of contacting bodies

In addition, planes 1 and 2 should be so chosen that:

$$\frac{1}{R_{a1}} + \frac{1}{R_{b1}} > \frac{1}{R_{a2}} + \frac{1}{R_{b2}} \qquad \text{Eq. A-7}$$

Plane 1 then determines the direction of the semi-minor axis of the contact area and plane 2 the direction of semi-major axis of the contact area.

The values of the functions μ and ν for use in Eqs. A-1 and A-2 depend on the conformity of the contacting bodies in the vicinity of the contact area as determined by the auxiliary angle γ

$$\cos\gamma = \frac{\frac{1}{R_{a1}} - \frac{1}{R_{a2}} + \frac{1}{R_{b1}} - \frac{1}{R_{b2}}}{\frac{1}{R_{a1}} + \frac{1}{R_{a2}} + \frac{1}{R_{b1}} + \frac{1}{R_{b2}}} \qquad \text{Eq. A-8}$$

Note that the denominator in the expression for $\cos\gamma$ is the same as that occurring under the radical in Eqs. A-3 and A-6.

μ and ν are related by another auxiliary angle ϵ, which depends on the shape of the contact ellipse.

$$\cos\gamma = 1 - \frac{2\,[K(\epsilon) - E(\epsilon)]\cot^2\epsilon}{E(\epsilon)} \qquad \text{Eq. A-9}$$

$$\nu = \sqrt[3]{\frac{2E(\epsilon)\cos\epsilon}{\pi}} \qquad \text{Eq. A-10}$$

where:

$$\cos\epsilon = \frac{\nu}{\mu} = \frac{b}{a} \qquad \text{Eq. A-11}$$

K (ϵ) and E (ϵ) are the complete elliptic integrals of the first and second order, having the modulus sin ϵ.

$$K(\epsilon) = \int_0^{\frac{\pi}{2}} \frac{d\phi}{\sqrt{1 - \sin^2\epsilon\,\sin^2\phi}} \qquad \text{Eq. A-12}$$

American Axle v. Neapco - IPR2025-00090
PET_AAM_1012-0346

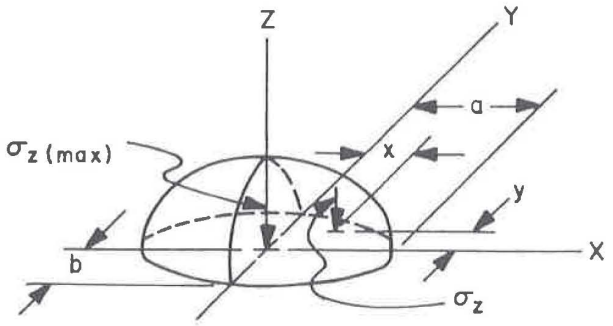


Fig. A-4 — Compressive stress distribution over elliptical contact surface

$$E(\epsilon) = \int_0^{\frac{\pi}{2}} \sqrt{1-\sin^2\epsilon\,\sin^2\phi}\;d\,\phi \qquad \text{Eq. A-13}$$

Since accurate tables of $K(\epsilon)$ and $E(\epsilon)$ are not always available, values of $K(\epsilon)$ and $E(\epsilon)$ correct to ten decimal places are given on Charts A-1 and A-2. Four place tables may also be found in Jahnke and Emde's, *Funktionentafeln*, 1943 edition.

By assuming a series of values of the modulus $\sin\epsilon$, corresponding values of $\cos\gamma$, μ and ν may be calculated by Eqs. A-9, A-10 and A-11.

Values of μ computed in this manner are plotted against corresponding values of $\cos\gamma$ in Charts A-3–A-17. Values of ν are plotted against corresponding values of $\cos\gamma$ in Charts A-18–A-27.

It must be emphasized that the semi-axes of the contact ellipse, a and b, are the projected semi-axes and are not measured along the curvature of the contact surface.

Compressive (Contact) Stress Analysis Procedure

Case of Two General Curved Surfaces

It is now possible to outline the steps to be followed in determining the size and shape of the contact area.

1. Determine the principal radii of curvature of the two bodies as indicated in Fig. A-1, choosing the signs of the radii of curvature in accordance with Fig. A-3. Check to see that Eq. A-7 is satisfied.
2. Obtain $\cos\gamma$ from Eq. A-8.
3. Obtain μ and ν from Charts A-3–A-17 and Charts A-18–A-27, respectively.
4. Determine g from Eq. A-6 if the bodies are of steel. If bodies are of different materials, use Eqs. A-4, A-5, and A-3.
5. Compute a and b by means of Eqs. A-1 and A-2, respectively.

Having determined the dimensions a and b of the contact area, the mean compressive stress S_m is:

$$S_m = \frac{P_o}{\pi ab} \qquad \text{Eq. A-14}$$

or, using Eqs. A-1, A-2, and A-6, for steel:

Eq. A-15

$$S_m = \frac{15079\left[\frac{1}{R_{a1}} + \frac{1}{R_{a2}} + \frac{1}{R_{b1}} + \frac{1}{R_{b2}}\right]^{2/3} P_o^{1/3}}{\mu\nu}$$

The actual distribution of the compressive stress over the surface of the elliptical contact area is proportional to the ordinates of a semi-ellipsoid of revolution erected on the contact area as a base as illustrated in Fig. A-4.

The compressive stress acting at any point (x, y) is:

$$\sigma_{z(x,y)} = \frac{3P_o}{2\,\pi\,ab}\sqrt{1-\frac{x^2}{a^2}-\frac{y^2}{b^2}} \qquad \text{Eq. A-16}$$

From this, it is seen that the maximum value of compressive stress occurs at the center of the contact area. Its value is:

$$\sigma_{z(max)} = \frac{3P_o}{2\,\pi\,ab} \qquad \text{Eq. A-17}$$

or, having the value of the mean compressive stress S_m from Eq. A-14 or A-15

$$\sigma_{z(max)} = \frac{3S_m}{2} \qquad \text{Eq. A-18}$$

Case of Two Cylinders

The previous equations apply to elliptical contact areas. The contact of two cylindrical surfaces along their elements requires somewhat different treatment.

Fig. A-5 shows two cylindrical bodies whose radii of curvature are R_a and R_b pressed together along a common element. The resulting contact area is a rectangle of width 2b and length L as shown in Fig. A-6.

If the total load is evenly distributed along the length L, the semi-width of the contact rectangle is:

$$b = \sqrt{\frac{P_o\,(\gamma_a + \gamma_b)}{\pi\,L\left(\frac{1}{R_a} + \frac{1}{R_b}\right)}} \qquad \text{Eq. A-19}$$

The signs of the radii of curvature R_a and R_b must be assigned in accordance with Fig. A-3. γ_a and γ_b are elastic constants defined by Eqs. A-4 and A-5.

When both bodies are of steel with $E = 29 \times 10^6$ psi and $\delta = 0.25$, the semi-width of the contact area is:

$$b = 0.00028692\sqrt{\frac{P_o}{L\left(\frac{1}{R_a} + \frac{1}{R_b}\right)}} \qquad \text{Eq. A-20}$$

The mean compressive stress is obtained by dividing the area of the contact rectangle into the total load.

American Axle v. Neapco - IPR2025-00090
PET_AAM_1012-0347

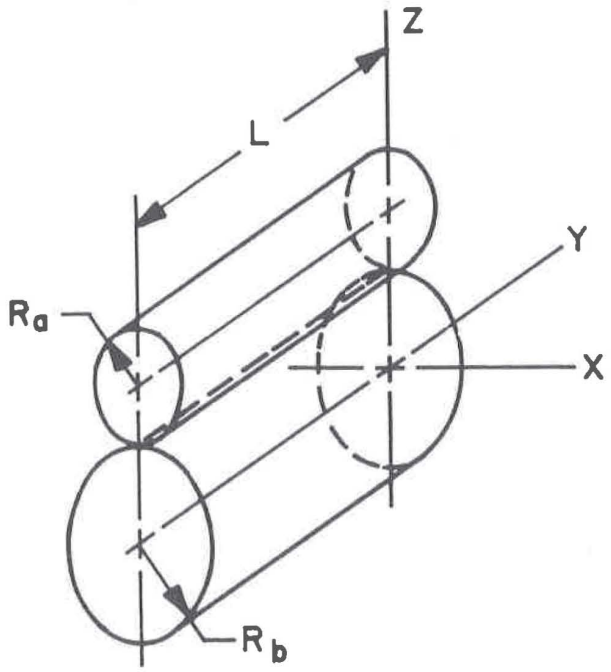


Fig. A-5 — Two cylinders in contact with parallel axes

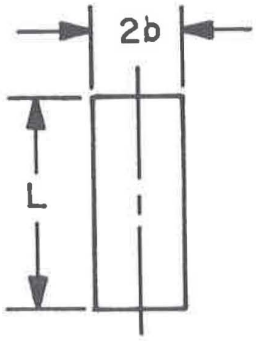


Fig. A-6 — Contact rectangle

$$S_m = \frac{P_o}{2bL} \qquad \text{Eq. A-21}$$

or, for steel:

$$S_m = 1742.6\sqrt{\frac{P_o}{L}\left(\frac{1}{R_a} + \frac{1}{R_b}\right)} \qquad \text{Eq. A-22}$$

The distribution of compressive stress over the surface of the contact rectangle is proportional to the ordinate of a semi-cylinder erected with the contact area as a base as shown in Fig. A-7. The compressive stress acting at the distance x from the center is:

$$\sigma_{z(x)} = \frac{2P_o}{\pi\, Lb}\sqrt{1 - \frac{x^2}{b^2}} \qquad \text{Eq. A-23}$$

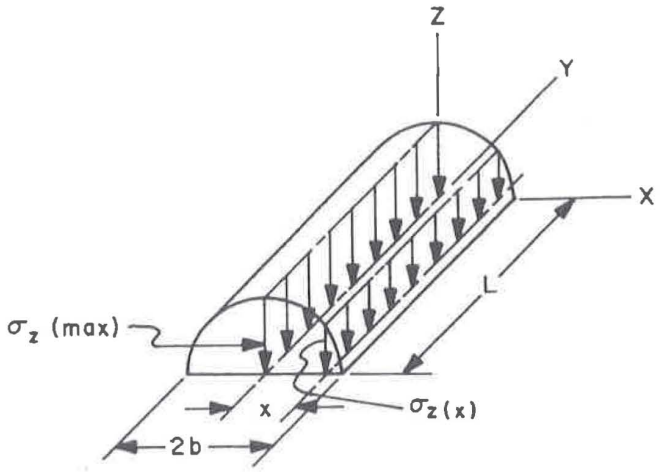


Fig. A-7 — Compressive stress distribution over rectangular contact surface

Thus, the maximum value of the compressive stress is along the center of the contact area and is:

$$\sigma_{z(max)} = \frac{2P_o}{\pi\, Lb} \qquad \text{Eq. A-24}$$

or, having the value of the mean compressive stress from Eqs. A-21 or A-22:

$$\sigma_{z(max)} = \frac{4\, S_m}{\pi} \qquad \text{Eq. A-25}$$

Thus, with the elliptical contact area, the maximum stress is 1.5 times the mean stress, whereas with a rectangular contact area, the maximum stress is but 1.2732 times the mean stress.

Case of Two Spheres

If, in Fig. A-1, $R_{a1} = R_{a2}$ and $R_{b1} = R_{b2}$, we have the case of two spherical bodies in contact, cos γ from Eq. A-8 is zero and $\mu = \nu = 1$. The contact area is a circle whose radius a is:

$$a = \sqrt[3]{\frac{3P_o\,(\lambda_a + \lambda_b)}{16\left(\frac{1}{R_a} + \frac{1}{R_b}\right)}} \qquad \text{Eq. A-26}$$

R_a and R_b are the radii of curvature of the two spherical bodies. The signs of the radii must be chosen in accordance with Fig. A-3. λ_a and λ_b are elastic constants defined by Eqs. A-4 and A-5.

When both bodies are of steel with $E = 29 \times 10^6$ psi and $\delta = 0.25$, the radius of the contact circle is:

$$a = 0.0036466\sqrt[3]{\frac{P_o}{\left(\frac{1}{R_a} + \frac{1}{R_b}\right)}} \qquad \text{Eq. A-27}$$

The mean compressive stress is:

$$S_m = \frac{P_o}{\pi\, a^2} \qquad \text{Eq. A-28}$$

American Axle v. Neapco - IPR2025-00090
PET_AAM_1012-0348

or, for steel:

$$S_m = 23\ 937\left(\frac{1}{R_a}+\frac{1}{R_b}\right)^{2/3} P_o^{1/3} \qquad \text{Eq. A-29}$$

The distribution of compressive stress over the contact circle is proportional to the ordinates of a hemisphere erected with the contact circle as a base. The compressive stress acting at any radius, r, from the center of the contact circle is:

$$\sigma_{z(r)} = \frac{3P_o}{2\pi a^2}\sqrt{1-\frac{r^2}{a^2}} \qquad \text{Eq. A-30}$$

The maximum value of compressive stress occurs at the center of the contact circle and is:

$$\sigma_{z(max)} = \frac{3P_o}{2\pi a^2} \qquad \text{Eq. A-31}$$

or, having the value of mean compressive stress, S_m from Eqs. A-28 or A-29:

$$\sigma_{z(max)} = \frac{3S_m}{2} \qquad \text{Eq. A-32}$$

Eqs. A-22 and A-29 for mean compressive stress were derived for steel bodies using a modulus of elasticity of E = 29 000 000 psi and Poisson's ratio of δ = 0.25. Most references quote for steel modulus of elasticity values ranging from 29 000 000-30 000 000 psi and a Poisson's ratio of 0.30. The reference *Elements of Strength of Materials*, by S. Timoshenko and G. H. MacCullough, D. Van Nostrand Company, Inc., New York, 1940, lists the Poisson's ratio of 0.25 used in this appendix as the value for an isotropic material. For most ferrous and nonferrous materials, the Poisson's ratio ranges from 0.25-0.35 and is considered a narrow range. Therefore, when these slightly varying values for modulus of elasticity and Poisson's ratio are used for steel, the resulting differences for mean compressive stress are generally negligible. For example, when using 30 000 000 instead of 29 000 000 psi and 0.30 instead of 0.25 for the modulus of elasticity and Poisson's ratio, respectively, the percentage increase is slightly over 3% for a needle roller on a trunnion, and slightly over 4% for a ball in a groove.

Subsurface Stresses

Case of Two General Curved Surfaces

The previous discussion has been limited to the compressive stresses which act normally on the contact surface. The material below the contact surface is also in a state of stress.

Considering an elementary particle at a depth z from the contact surface and located on the Z axis as shown in Fig. A-8, we find that the particle is acted upon by a total stress which may be resolved into three principal stresses, σ_x, σ_y, and σ_z acting as shown in Fig. A-8.

The system of coordinates chosen with the origin at the center of the contact area, the X axis indicating the direction of the major axis of the ellipse and the Y axis the minor. The Z axis is drawn perpendicular to the pressure surface. We limit discussion to those stresses existing along the Z axis since maximum values of the principal stresses occur there.

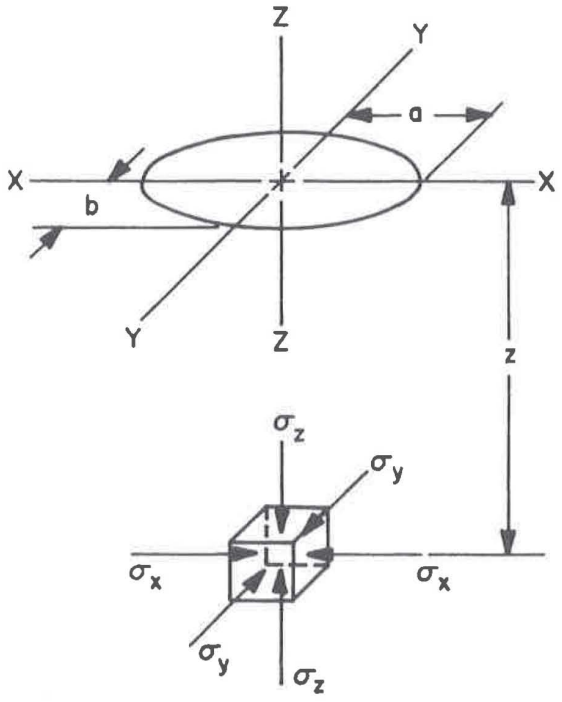


Fig. A-8 — Elementary subsurface particle below contact surface

The following method of subsurface stress determination is an adaptation of that devised by Thomas and Hoersch *(Bulletin 212,* Engineering Experiment Station, University of Illinois, 1930).

It is assumed that two solid elastic bodies, Fig. A-1, have been pressed together with the load P_o. The principal radii of curvature, R_{a1}, R_{a2}, R_{b1}, and R_{b2} have been chosen in accordance with Eq. A-7, and the signs of the radii are in accordance with Fig. A-3.

It is also assumed that semi-axes of the contact ellipse, a and b, have been determined as previously outlined, as has the maximum compressive stress, $\sigma_{z(max)}$, at the center of the contact area.

Let:

$$k = \frac{b}{a} = \cos\epsilon \qquad \text{Eq. A-33}$$

$$(k')^2 = 1 - k^2 \qquad \text{Eq. A-34}$$

$$B = \frac{1}{2}\left(\frac{1}{R_{a1}}+\frac{1}{R_{b1}}\right) \qquad \text{Eq. A-35}$$

$$A = \frac{1}{2}\left(\frac{1}{R_{a2}}+\frac{1}{R_{b2}}\right) \qquad \text{Eq. A-36}$$

American Axle v. Neapco - IPR2025-00090
PET_AAM_1012-0349

In accordance with Eq. A-7, B > A so that plane 1 determines the direction of the Y (minor) axis and plane 2 the direction of the X (major) axis in Fig. A-8.

$$\Lambda = \left| \frac{1 - \delta_a^2}{E_a} + \frac{1 - \delta_b^2}{E_b} \right| \frac{1}{(A+B)} \qquad \text{Eq. A-37}$$

If both bodies are of steel with Poisson's ratio $\delta = 0.25$ and $E = 29 \times 10^6$ psi:

$$\Lambda = \frac{6.4655 \times 10^{-8}}{(A+B)} = \frac{12.9310 \times 10^{-8}}{\sum \frac{1}{R}} \qquad \text{Eq. A-38}$$

Let z be the distance along the Z axis from the contact surface to the stressed particle under consideration and obtain:

$$\xi = \cot \phi = \frac{z}{a} = \frac{kz}{b} \qquad \text{Eq. A-39}$$

$$\gamma = \sqrt{\frac{k^2+\xi^2}{1+\xi^2}} \qquad \text{Eq. A-40}$$

$$M = \frac{2k}{k'^2 E(k')} = \frac{2\cos \epsilon}{\sin^2 \epsilon \, E(k')} \qquad \text{Eq. A-41}$$

where E(k') is the complete elliptic integral of the second order having the modulus $k' = \sin \epsilon$ where $\cos \epsilon = k$ from Eq. A-33.

$$E(k') = \int_0^{\frac{\pi}{2}} \sqrt{1 - k'^2 \sin^2 \theta} \; d\theta \qquad \text{Eq. A-42}$$

Also required are:

$$\Omega_x = - \frac{1-\gamma}{2} + \xi \left[F(\phi,k') - E(\phi,k') \right] \qquad \text{Eq. A-43}$$

$$\Omega'_x = - \frac{\gamma}{k^2} + 1 + \xi \left[\frac{E(\phi,k')}{k^2} - F(\phi,k') \right] \qquad \text{Eq. A-44}$$

$$\Omega_y = \frac{1}{2\gamma} + \frac{1}{2} - \frac{\gamma}{k^2} + \xi \left[\frac{E(\phi,k')}{k^2} - F(\phi,k') \right] \qquad \text{Eq. A-45}$$

$$\Omega'_y = - 1 + \gamma + \xi \left[F(\phi,k') - E(\phi,k') \right] \qquad \text{Eq. A-46}$$

where $F(\phi, k')$ and $E(\phi, k')$ are incomplete elliptic integrals of the first and second order, respectively, values of which are to be found in Jahnke and Emde's, *Funktionentafeln,* and in the *Smithsonian Mathematical Formulae* and *Tables of Elliptic Functions*.

By means of the above equations, the three principal stresses, σ_x, σ_y, and σ_z at any depth, $z = b\frac{\xi}{k}$ below the contact surface may be computed as follows:

$$\frac{\Lambda\sigma_x}{b} = M(\Omega_x + \delta\Omega'_x) \qquad \text{Eq. A-47}$$

$$\frac{\Lambda\sigma_y}{b} = M(\Omega_y + \delta\Omega'_y) \qquad \text{Eq. A-48}$$

$$\frac{\Lambda\sigma_z}{b} = - \frac{M}{2} \left(\frac{1}{\gamma} - \gamma \right) \qquad \text{Eq. A-49}$$

In the previous equations, compressive stress is considered negative and tensile stress positive.

For any given value of $\frac{b}{a}$ the three principal stresses may be plotted against depth z from the contact surface. The difference between any two of the principal stresses may be obtained graphically, and the maximum shear stress, equal to one half the maximum difference between any two principal stresses, obtained directly. The location of the point of maximum shear stress, with respect to the contact surface, is indicated directly on such a plot. The maximum shear stress will be found to depend on the stress difference $\frac{1}{2}(\sigma_z - \sigma_y)$.

Case of Two Spheres

Consider that the contact area is circular, k = 1 and b = a, and the evaluation of the principal stresses no longer involves elliptic functions. In this case:

$$\frac{\Lambda\sigma_x}{b} = \frac{\Lambda\sigma_y}{b} = \frac{2}{\pi} \left[(1+\delta)(-1 + \phi \cot \phi) + \frac{1}{2} \sin^2 \phi \right] \qquad \text{Eq. A-50}$$

$$\frac{\Lambda\sigma_z}{b} = - \frac{2}{\pi} \sin^2 \phi \qquad \text{Eq. A-51}$$

The point of maximum shear in this case lies at $Z_1 = 0.467$ b below the contact surface. The value of the maximum shear stress is:

$$S_s = - 0.205 \frac{b}{\Lambda} \qquad \text{Eq. A-52}$$

Case of Two Cylinders

When the contact area is rectangular, as for a roller contacting along an element, k = 0 and the equations for the principal stresses become:

$$\frac{\Lambda\sigma_x}{b} = - 2\delta \left[\sqrt{1 + \left(\frac{z}{b}\right)^2} - \frac{z}{b} \right] \qquad \text{Eq. A-53}$$

American Axle v. Neapco - IPR2025-00090
PET_AAM_1012-0350

$$\frac{\Lambda\sigma_y}{b} = -\frac{\left[\sqrt{1+\left(\frac{z}{b}\right)^2}-\frac{z}{b}\right]^2}{\sqrt{1+\left(\frac{z}{b}\right)^2}} \qquad \text{Eq. A-54}$$

$$\frac{\Lambda\sigma_z}{b} = -\frac{1}{\sqrt{1+\left(\frac{z}{b}\right)^2}} \qquad \text{Eq. A-55}$$

In this case, the maximum shear stress lies at $Z_1 = 0.7861$ b below the contact surface and is:

$$S_s = -0.30025\ \frac{b}{\Lambda} \qquad \text{Eq. A-56}$$

Subsurface Stress Analysis Procedure

To expedite the solution of subsurface stresses, the following charts have been prepared.

Charts A-28, A-29, and A-30 show, respectively, the values of the principal stresses σ_x, σ_y, and σ_z as ratios to the maximum compressive stress $\sigma_{z(max)}$ at the center of the contact area, for all values of the ratio $\frac{b}{a}$ and for various depths $\frac{z}{b}$ below the contact surface.

Chart A-31 shows the ratio of the maximum shear stress S_s to the maximum compressive stress at the center of the contact area, and also the depth $\frac{Z_1}{b}$ of the point of maximum shear stress below the surface.

The procedure to be followed in analyzing subsurface stresses is as follows:

1. Determine the dimensions of the contact area, a and b, and obtain the ratio $\frac{b}{a}$. Note that $\frac{b}{a}$ is unity for a circular contact area and zero for a rectangular area.
2. Determine $\sigma_{z(max)}$ the maximum compressive stress at the center of the contact surface.
3. From charts A-28, A-29, and A-30, at the proper value of $\frac{b}{a}$ and for assumed values of $\frac{z}{b}$ the depth from the contact surface, obtain $\frac{\sigma_x}{\sigma_{z(max)}}$, $\frac{\sigma_y}{\sigma_{z(max)}}$, and $\frac{\sigma_z}{\sigma_{z(max)}}$. Multiply these values by the above obtained value of $\sigma_{z(max)}$ to obtain the principal stresses.
4. From Chart A-31, obtain the depth $\frac{Z_1}{b}$ to the point of maximum shear stress. Multiply by b to obtain Z_1.
5. From Chart A-31, obtain $\frac{S_s}{\sigma_{z(max)}}$. Multiply by $\sigma_{z(max)}$ to obtain the shear stress.

Stress and Strength Gradients Along the Load Axis Including Subsurface Shear and Residual Stress Effects

With the previous subsurface stress analysis procedure, it is possible to compute the three principal stresses as well as the three maximum shear stresses along the load or Z axis of two contacting bodies. This study will provide a knowledge of the elastic stress distribution within the contact zone to any desired depth z. Fig. A-9 shows a plot of a typical elastic stress distribution along the Z axis for two contacting cylinders with parallel axes. Of particular interest is the value of highest maximum shear stress τ_{yz} and its depth Z_1 below the surface. This depth of maximum shear stress must be considered in case depth determination of typical surface hardened rolling element bearing components.

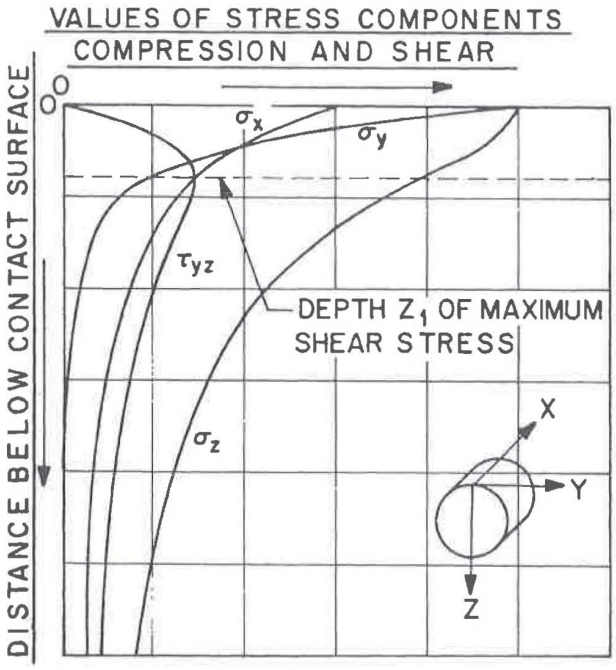


Fig. A-9 — Typical elastic stresses along load or Z axis

The actual load carrying capability of bodies subjected to contact loading depends upon more than the nominal elastic stresses shown in Fig. A-9 and computed from the Hertz equations. Surface sliding (or even a tendency to slide) causes shear loading on the contacting surfaces; sliding creates frictional heat with resulting thermal stresses and altered material properties; lubricating fluid films alter the surface loadings; working stresses are usually sufficiently high so that localized yielding occurs, giving rise to residual stresses; various component forming or processing procedures as well as surface hardening heat treatment result in additional important residual stresses; etc. A detailed discussion of these factors and their effects can be found in various references.

When a cylindrical component is surface hardened after carburizing, for example, the residual stresses resulting from this heat treatment can be plotted on axes similar to those used in Fig. A-9. The general shapes of the resulting curves are as shown in Fig. A-10, and it should be noted that tensile as well as compressive residual stress components exist below the surface. The curves are plotted with stress as the abscissa and depth below the surface as the ordinate. Also shown in this figure is the hardness gradient curve for this component, but it is plotted with hardness as the abscissa and depth as the ordinate.

When the elastic principal stresses σ_x, σ_y, and σ_z in Fig. A-9 are added to the residual stresses σ_{xr}, σ_{yr}, and σ_{zr} in Fig. A-10, the resulting principal stresses when plotted will be as

American Axle v. Neapco - IPR2025-00090
PET_AAM_1012-0351

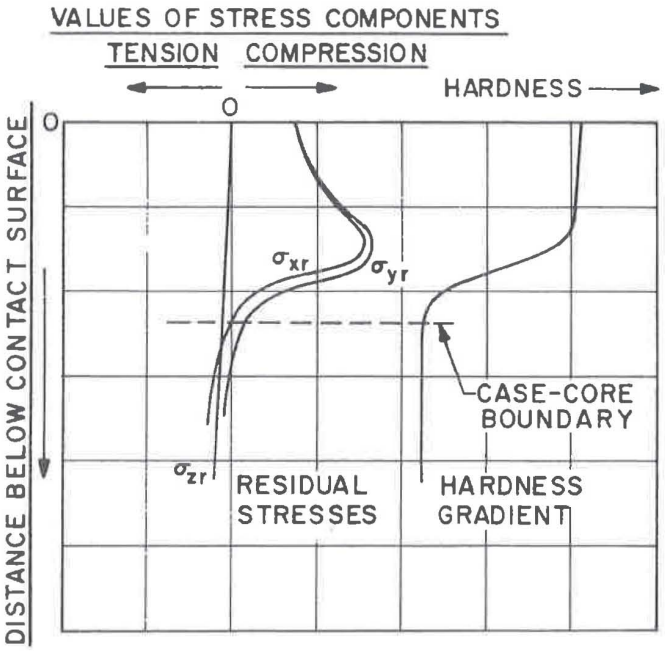


Fig. A-10 — Typical residual stress components and hardness gradient for a carburized and hardened cylindrical bar

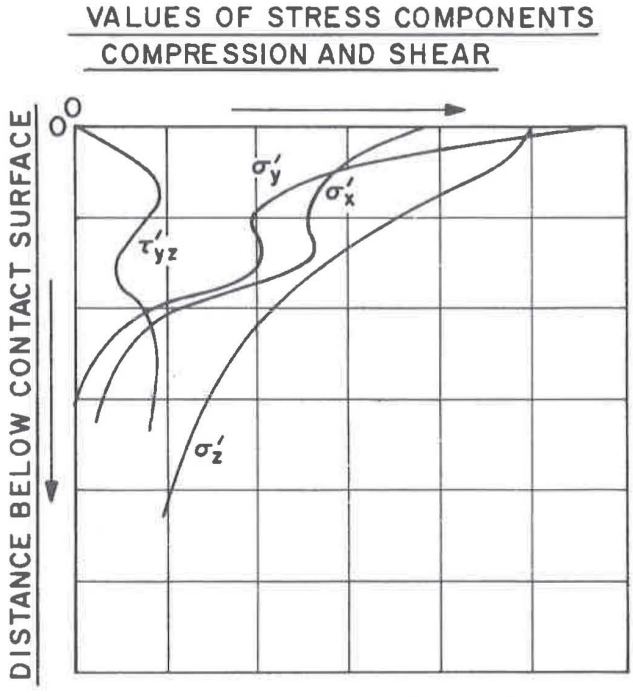


Fig. A-11 — Typical resultant stresses due to elastic and residual stresses

shown in Fig. A-11. The effect of the residual stresses on the highest maximum shear stress can also be plotted as shown in Fig. A-11, and it is noted that this shear stress has two mathematical maximum points.

For a given component, the shear yield strength can be estimated from the hardness gradient curve shown in Fig.

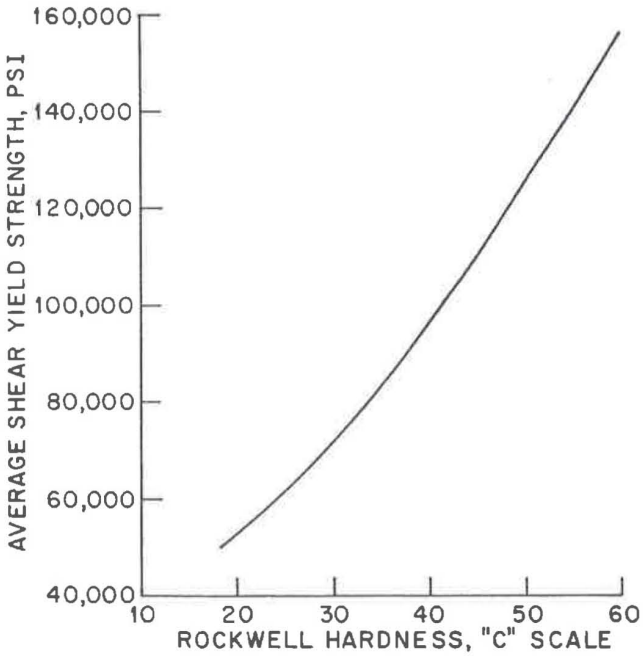


Fig. A-12 — Average shear yield strength versus Rockwell "C" hardness

A-10. Fig. A-12 shows a curve of the average shear yield strength versus hardness in Rockwell "C" values. The shear yield strength curve can then be plotted as shown in Fig. A-13. To facilitate comparison with the previously plotted resultant maximum shear stress in Fig. A-11, the shear yield strength is plotted as the abscissa, and the depth below the surface as the ordinate. When the maximum shear stress curve of Fig. A-11 and the shear yield strength curve of Fig. A-13 are plotted to the same coordinate axes, the result is shown in Fig. A-14. Although these are generalized curves, their individual shapes, as well as their relationship to each other, are typical for two contacting cylinders with parallel axes.

The shear stress curve represents a certain load, and when higher load values are applied to the component, the resulting shear stresses will more closely approach the shear yield strength curve as can be seen in Fig. A-14. Therefore, a minimum depth of case and case hardness is necessary to prevent a subsurface shear failure. The shear yield strength curve has a pronounced "knee" at a depth where the hardened case meets the softer core material. In Fig. A-10, it can be noted that at about the depth where the case and core meet, the compressive residual stresses are small enough to be negligible. This is so because in the case-core boundary region a reversal in sign of the residual stress occurs from compression in the case to tension in the core. Therefore, at the depth of the case-core boundary, the shear stresses produced by the applied load are not affected appreciably by the residual stresses.

Thus far, no mention was made of the resultant principal stresses σ_x', σ_y', and σ_z' shown in Fig. A-11. These values are a maximum at the surface where the tri-axial stress state is in

American Axle v. Neapco - IPR2025-00090
PET_AAM_1012-0352

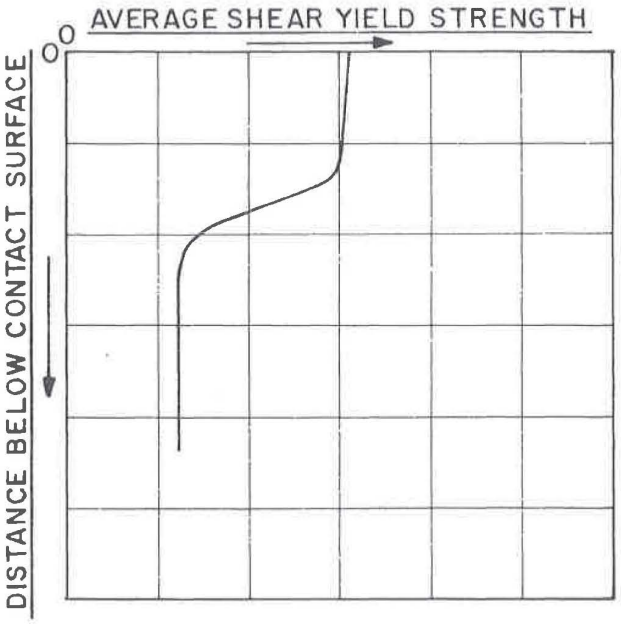


Fig. A-13 — Typical shear yield strength curve for a carburized and hardened cylindrical bar

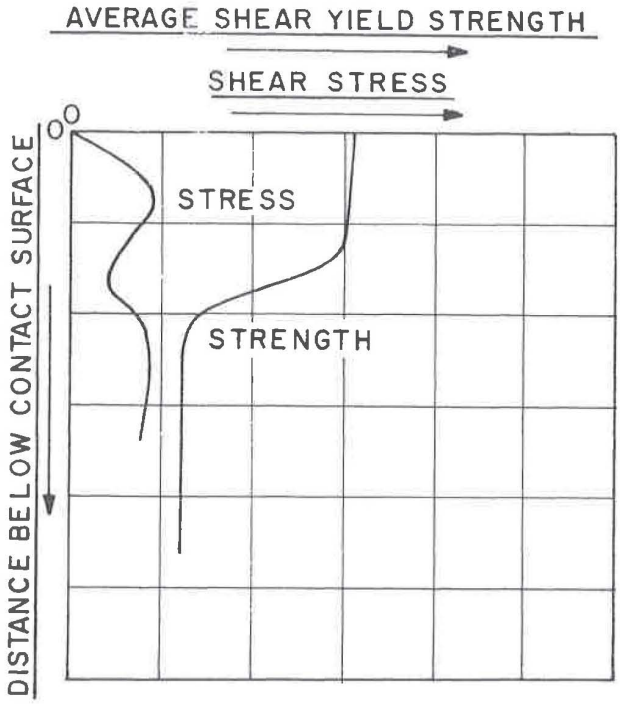


Fig. A-14 — Subsurface shear stress compared to shear yield strength for a carburized and hardened cylindrical bar

compression. This stress system is usually not conducive to plastic flow, and failure due to compression alone is unusual, although possible.

Because of the obvious complexities associated with an analysis procedure involving more than the nominal elastic stresses, the mean compressive (Hertz contact) stress is often used as an "index" of contact loading severity. For example, using the Hertz equations, one can compute the mean compressive stress corresponding to a known test or application situation giving borderline failure. This value can then be used as a design guide for evaluating or comparing components having loading conditions which are sufficiently similar to the known test condition.

Allowable Limits of Compressive (Contact) Stress

It has been repeatedly confirmed in laboratory tests that when a static load corresponding to 500 000-525 000 psi mean compressive (Hertz contact) stress is applied by a steel ball on a ground and polished steel plate, a brinell spot of approximately 0.0001 of the ball diameter results on the plate surface. The surface hardness of both ball and plate is R_c64, the material is SAE 52100, and the contacting surfaces are dry in this ideal test condition.

Most universal joint constructions employ rolling elements, such as needle rollers or balls, which are usually in the typical R_c60-64 and R_c62-65 hardness range, respectively. Because of varying component design characteristics, material usage, and processing procedures employed, the bearing surfaces, raceways, or ball grooves of the mating joint components are at times somewhat lower in surface hardness and have less smoother than ideal surface finishes.

Carburizing low carbon alloy steels can yield a surface hardness of R_c60 minimum, while induction hardened plain medium carbon steels may result in a somewhat lower hardness depending on the specific material used. However, a surface hardness of R_c60 minimum is readily attainable with the proper induction hardenable steel and heat treating procedure.

If a surface hardening procedure such as carburizing or induction hardening is used, the case depth and hardness should be adequate as previously indicated, and without soft spots. The core structure, in addition to supporting the case, should have an adequate hardness range which will withstand the various static, fatigue, and impact loading requirements that the particular component may be subjected to. Depending on the type of low carbon alloy steel and section size used for a carburized component, the normal core hardness range may be from as low as R_c20 approximately at the center, to approximately R_c42 just below the case. Unlike carburized components, when induction hardening a plain medium carbon steel component, the core structure must be initially developed to a satisfactory hardness range, depending on the type of steel used, for optimum surface and case hardening response. When any component of a given section size is surface hardened to a given case depth by either of the two methods described, a sufficient amount of core area in the proper hardness range is desirable to provide good strength, toughness, and ductility.

With regard to surface finish, universal joints employing needle rollers have generally used smoothly ground bearing surfaces with a roughness height of less than 35 microinches (arithmetical average). It is believed by bearing authorities

American Axle v. Neapco - IPR2025-00090
PET_AAM_1012-0353

that the finer finish means better bearing performance, and insofar as it diminishes the progress of fretting corrosion, results in longer bearing life.

In universal joints employing balls, the ball grooves have usually been finish ground after surface hardening to a roughness height of less than 35 microinches (arithmetical average). Recently, certain ball type joints have had their ball grooves, or raceways, finished before surface hardening by broaching, forming, or by other processing means. The resulting surface finish from broaching, especially, is generally not as smooth as a ground surface, and at this time, the effect of the rougher finish on the Hertz contact stress as well as joint life has not been established.

Needle rollers or balls used in the various joints function similar to oscillatory bearing rolling elements with varying degrees of sliding present in ball type joint designs. Lubrication must be provided to ensure adequate life, low operating temperatures, and other desired functional characteristics. For a given bearing load and angle of oscillation, especially small oscillatory motions, the best deterrents to fretting corrosion and false brinelling are relatively low Hertz contact stresses and good lubrication. It would be ideal if the bearing surfaces could be kept constantly wetted with lubricant, and if the products of fretting corrosion could be carried away immediately after formation, but this requires oil lubrication in large quantities which is impractical in joints for most vehicle applications. Therefore, a certain level of compressive (Hertz contact) stress between the rolling element and the bearing raceway should not be exceeded to prevent fretting corrosion and false brinelling when good lubrication is present.

It has been the practice to generally express the Hertz contact stress in terms of the mean compressive or mean Hertz contact stress. For a given contact surface, it was previously shown that the maximum value of the compressive stress occurs at the center of an elliptical contact area and along the longitudinal centerline of a rectangular contact area. For an elliptical contact area the maximum stress is 1.5 times the mean stress and for a rectangular contact area the maximum stress is 1.2732 times the mean stress.

For universal joint design, the recommended level of the Hertz contact stress can vary substantially with the particular type of joint being considered. Also, based on experience with a given joint design and when optimized joint design and processing procedures are employed, levels of contact stress higher than those recommended can be successfully utilized.

For Cardan and double Cardan joints, the mean contact stress between the needle rollers and the cross trunnions can be 400 000 psi or higher at the maximum applied torque. As previously indicated, the upper limit of the contact stress will depend on the specific joint design and processing procedures.

The application of needle rollers in ball and trunnion or tripot type joints, however, requires a reduction in the allowable contact stress at the trunnion surface of the pin or spider, respectively. This reduction is required due to the axial sliding effects between the bore of the ball and needle rollers and between the needle rollers and the trunnion surface when the joint operates at an angle. It is recommended that the mean contact stress on the trunnion be limited to 350 000 psi maximum.

In both the ball and trunnion and tripot joints, the mean contact stress between the ball and housing ball bore should not exceed approximately 260 000 psi for optimum wear characteristics. For conventional ball type constant velocity joints, the ball-to-groove mean contact stress can be as high as 325 000 psi approximately.

In rolling element spline mechanisms, the mean contact stress can be as high as 400 000 psi or higher. This higher stress level is permissible since relatively little sliding or skidding occurs between the rolling element and the raceway as compared to the significant amount of sliding which occurs in certain types of universal joints.

For these allowable stress limits, the surface hardness should be R_c60 minimum, and the contacting components should have proper metallurgical structures. Experience in rolling element bearings has indicated that in general optimum bearing performance can be obtained when the mating raceways employ R_c hardness values averaging approximately two points lower than the rolling elements.

If the surface hardness is less than R_c60 for a ball race, or less than R_c58 for a needle roller race, the allowable mean contact or compressive stresses previously indicated are somewhat less with a resulting reduction in load capacity of the bearing. Some bearing manufacturers have established reductions of static as well as dynamic capacity for given lower surface hardness levels. This data can be used with a reasonable degree of accuracy in computing universal joint load capacity when lower than optimum bearing surface hardnesses are used.

As with conventional rotating or oscillatory rolling element bearings, universal joints with rolling elements do not exhibit a definite endurance or fatigue limit. *Appendix B* lists useful load-speed-life-stress relationships for various rolling elements. If desired, universal joint life can be conveniently shown on a chart where either the torque load or the maximum or the mean compressive (Hertz contact) stress can be plotted versus life in hours with the joint operating at a given speed and joint angle.

Determination of Adequate Carburized Case Depth

The first consideration for carburized case depth computation is determining the depth Z_1 to the point of maximum subsurface shear as shown in Fig. A-9. A knowledge of the location of this depth can serve as a very useful purpose in design, since it can be predicted whether a subsurface failure can take place when two bodies of known hardnesses or hardness gradients are pressed together under a given load.

If a steel component has a carburized surface hardness of R_c60 minimum, it has been generally accepted that the depth of the required effective case must be approximately $2Z_1$ for no subsurface shear (static yielding or fatigue) failure to

American Axle v. Neapco - IPR2025-00090
PET_AAM_1012-0354

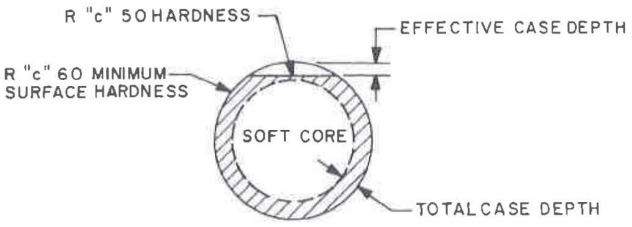


Fig. A-15 — Effective carburized case depth

occur. Effective case depth is defined as the depth where the case hardness is R_c50 as illustrated in Fig. A-15.

Many bearing authorities consider this depth to be approximately two thirds of the total applied carburized case. In bearing applications, this minimum effective case depth should not be less than 0.010 in. Therefore, for a typical universal joint component with a contact load application where Z_1 is 0.005 in, the total required carburized case depth would be $3Z_1 = 3 \times 0.005 = 0.015$ in. A typical specified case depth of 0.015–0.025 in with a minimum surface hardness of R_c60 would generally be considered satisfactory. This depth is based on contact load computation only, and would also be sufficient to allow for the residual stress effects previously indicated. However, when a joint component under contact loading by rolling elements is subjected to additional loading modes, such as bending or torsion, additional case depth considerations generally must be made in order to meet the application requirements.

For example, the cross trunnions of a Cardan universal joint, the pin of a ball and trunnion universal joint, or the spider trunnions of a tripot universal joint are subjected to high bending loads. In addition to the deflection caused by bending, a relatively thin case hardened surface can also deflect depending on the normal force exerted by the rolling element on the contact area and the hardness of the relatively soft core immediately beneath this surface. In order to ensure sub-surface strength to support the extremely hard case, a gradual case-to-core transition zone is desirable. Therefore, in order to provide the necessary ultimate and fatigue strength, and bearing life, certain joint components must be surface hardened with an adequate case depth, which can be substantially deeper than that computed for contact loading only.

In another example, a typical ball type universal joint outer race is assumed to be surface hardened by either carburizing a low carbon alloy steel or induction hardening a plain medium carbon steel. Both methods of heat treatment must provide an adequate case depth and the necessary surface hardness to meet the various functional requirements such as the contact loading in the ball grooves and the torsional strength. For a carburized outer race, the necessary case depth in the ball grooves based on contact load computations in general will also be adequate for the torsional strength of the component. This is because the case depth and R_c60 minimum surface hardness obtained is quite uniform on all surfaces. For an induction hardened outer race, the total case depth or heat affected depth obtained is first of all deeper due to the difference in process characteristics. Also, when induction hardening only necessary or functional areas such as the ball grooves, the spherical or cylindrical inner bearing surface and other selected surfaces are surface hardened to a desired case depth and R_c60 minimum surface hardness, or to other adequate surface hardness levels depending on the functional requirements of a particular surface. Certain areas are, therefore, not affected by this heat treatment process and depending on the geometry of the component and the material employed, a deeper case depth is obtained in certain areas or may be often desirable or necessary to provide the ultimate and fatigue strength equivalent to a component which is carburized uniformly all over.

References

1. H. Hertz, "Über die Berührung fester elastischer Körper (The Contact of Solid Elastic Bodies)," *Journal für die Reine und Angewandte Mathematik (Journal for Pure and Applied Mathematics)*, Berlin, 1881, pp. 156-171. Über die Berührung fester elastischer Körper und über die Härte (The Contact of Solid Elastic Bodies and Their Hardnesses), Berlin, 1882; Reprinted in H. Hertz, Gesammelte Werke (Collected Works), Vol. 1, pp. 155-173, 174-196, Leipzig, 1895, or the English translation H. Hertz, Miscellaneous Papers, translated by D. E. Jones and G. A. Schott, pp. 146-162, 163-183, London: Macmillan and Co., Ltd., 1896.

2. A. B. Jones, "Analysis of Stresses and Deflections," *New Departure*, Vol. I and II, GMC, 1946.*

3. F. B. Seely and J. O. Smith, *Advanced Mechanics of Materials*, 2nd ed., New York: John Wiley and Sons, Inc., 1952.

4. S. Timoshenko, *Strength of Materials, Part II*, 3rd ed. New Jersey: D. Van Nostrand Co., Inc., 1956.

5. H. A. Rothbart, *Cams-Design, Dynamics and Accuracy*, New York: John Wiley and Sons, Inc., 1956.

6. A. Palmgren, *Ball and Roller Bearing Engineering*, 3rd ed. Pennsylvania: SKF Industries, Inc., 1959.

7. R. Pedersen and S. L. Rice, *"Case Crushing" of Carburizing and Hardened Gears*, SAE Paper 220B, 1960.

8. W. Flügge, *Handbook of Engineering Mechanics*, 1st ed. New York: McGraw-Hill Book Co., 1962.

9. R. J. Roark, *Formulas for Stress and Strain*, 4th ed. New York: McGraw-Hill Book Co., 1965.

10. R. C. Juvinall, *Engineering Considerations of Stress, Strain, and Strength*, New York: McGraw-Hill Book Co., 1967.

11. S. P. Timoshenko and J. N. Goodier, *Theory of Elasticity*, 3rd ed., New York: McGraw-Hill Book Co., 1970.

Note: A detailed list of references is given in J. L. Lubkin, "Contact Problems," Chapter 42 of W. Flügge, Editor, *Handbook of Engineering Mechanics* listed above.

*Text material and charts used with permission of New Departure - Hyatt Bearings Div., GMC.

American Axle v. Neapco - IPR2025-00090
PET_AAM_1012-0355

Chart A-1

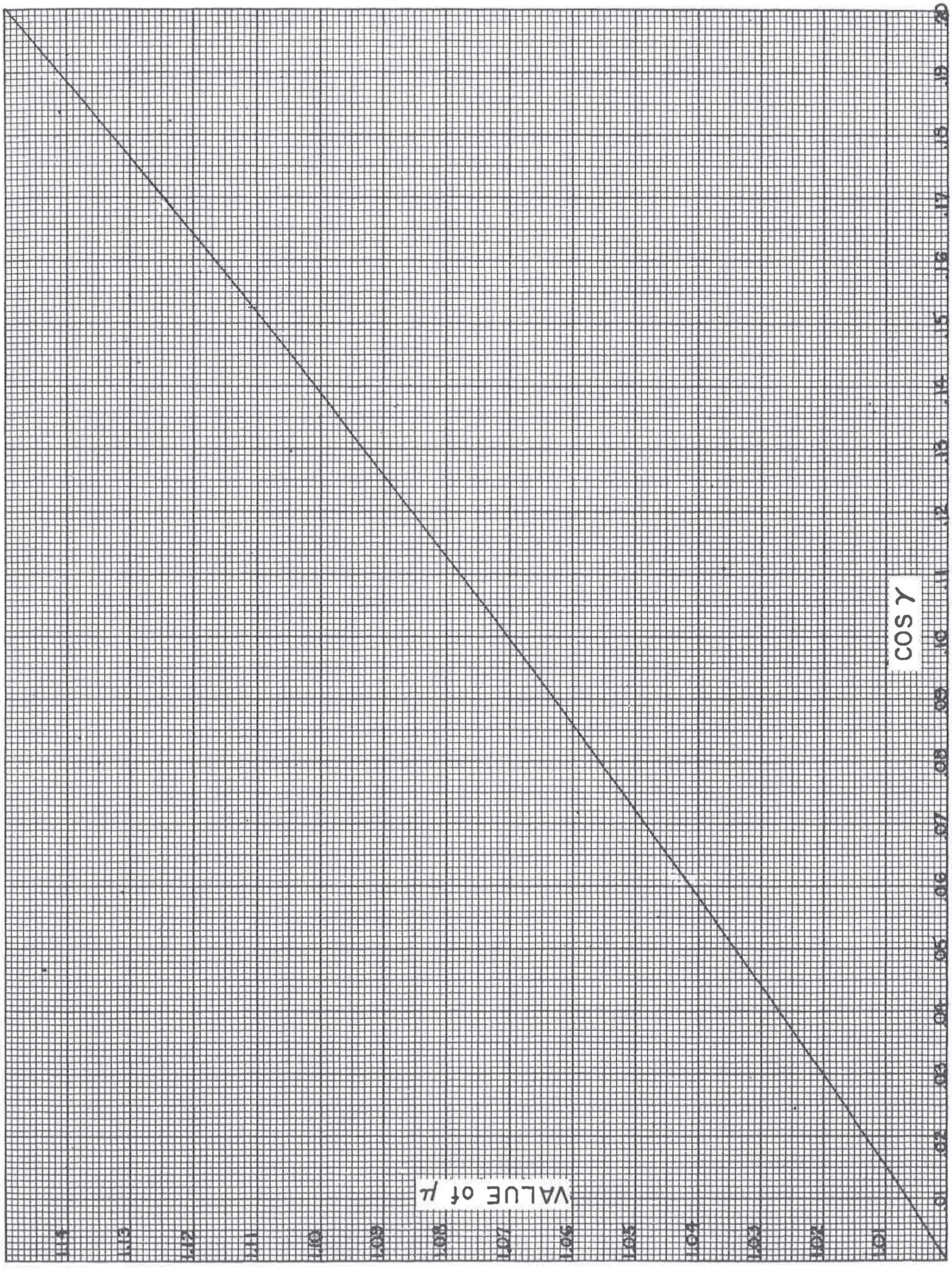
k^2	K	K′	k_1^2
0.00	1.5707 96327	∞	1.00
0.01	1.5747 45562	3.6956 37365	0.99
0.02	1.5787 39913	3.3541 41447	0.98
0.03	1.5827 80342	3.1558 74948	0.97
0.04	1.5868 67848	3.0161 12492	0.96
0.05	1.5910 03453	2.9083 37249	0.95
0.06	1.5951 88221	2.8207 52497	0.94
0.07	1.5994 23245	2.7470 73005	0.93
0.08	1.6037 09654	2.6835 51406	0.92
0.09	1.6080 48620	2.6277 73333	0.91
0.10	1.6124 41348	2.5780 92113	0.90
0.11	1.6168 89091	2.5333 34546	0.89
0.12	1.6213 93138	2.4926 35323	0.88
0.13	1.6259 54829	2.4553 38029	0.87
0.14	1.6305 75549	2.4209 32960	0.86
0.15	1.6352 56733	2.3890 16487	0.85
0.16	1.6399 99866	2.3592 63555	0.84
0.17	1.6448 06491	2.3314 08569	0.83
0.18	1.6496 78206	2.3052 31736	0.82
0.19	1.6546 16667	2.2805 49138	0.81
0.20	1.6596 23598	2.2572 05327	0.80
0.21	1.6647 00787	2.2350 67756	0.79
0.22	1.6698 50087	2.2140 22499	0.78
0.23	1.6750 73429	2.1939 70926	0.77
0.24	1.6803 72823	2.1748 27090	0.76
0.25	1.6857 50355	2.1565 15648	0.75
0.26	1.6912 08200	2.1389 70185	0.74
0.27	1.6967 48620	2.1221 31864	0.73
0.28	1.7023 73978	2.1059 48320	0.72
0.29	1.7080 86731	2.0903 72747	0.71
0.30	1.7138 89448	2.0753 63136	0.70
0.31	1.7197 84808	2.0608 81647	0.69
0.32	1.7257 75610	2.0468 94078	0.68
0.33	1.7318 64779	2.0333 69409	0.67
0.34	1.7380 55373	2.0202 79429	0.66
0.35	1.7443 50597	2.0075 98398	0.65
0.36	1.7507 53804	1.9953 02778	0.64
0.37	1.7572 68506	1.9833 70981	0.63
0.38	1.7638 98389	1.9717 83163	0.62
0.39	1.7706 47324	1.9605 21045	0.61
0.40	1.7775 19372	1.9495 67750	0.60
0.41	1.7845 18805	1.9389 07665	0.59
0.42	1.7916 50116	1.9285 26319	0.58
0.43	1.7989 18040	1.9184 10270	0.57
0.44	1.8063 27560	1.9085 47016	0.56
0.45	1.8138 83937	1.8989 24910	0.55
0.46	1.8215 92727	1.8895 33080	0.54
0.47	1.8294 59798	1.8803 61360	0.53
0.48	1.8374 91364	1.8714 00241	0.52
0.49	1.8456 93998	1.8626 40803	0.51
0.50	1.8540 74677	1.8540 74677	0.50
K_1^2	K′	K	k^2

Chart A-2

k^2	E	E′	k_1^2
0.00	1.5707 96327	1.0000 00000	1.00
0.01	1.5668 61942	1.0159 93546	0.99
0.02	1.5629 12645	1.0285 94520	0.98
0.03	1.5589 48244	1.0399 46861	0.97
0.04	1.5549 68546	1.0505 02227	0.96
0.05	1.5509 73352	1.0604 73728	0.95
0.06	1.5469 62456	1.0699 86130	0.94
0.07	1.5429 35653	1.0791 21407	0.93
0.08	1.5388 92730	1.0879 37503	0.92
0.09	1.5348 33465	1.0964 77517	0.91
0.10	1.5307 57637	1.1047 74733	0.90
0.11	1.5266 65017	1.1128 55607	0.89
0.12	1.5225 55369	1.1207 41661	0.88
0.13	1.5184 28454	1.1284 50735	0.87
0.14	1.5142 84027	1.1359 97843	0.86
0.15	1.5101 21831	1.1433 95792	0.85
0.16	1.5059 41612	1.1506 55629	0.84
0.17	1.5017 43101	1.1577 86979	0.83
0.18	1.4975 26026	1.1647 98293	0.82
0.19	1.4932 90109	1.1716 97053	0.81
0.20	1.4890 35058	1.1784 89924	0.80
0.21	1.4847 60581	1.1851 82883	0.79
0.22	1.4804 66375	1.1917 81311	0.78
0.23	1.4761 52126	1.1982 90087	0.77
0.24	1.4718 17514	1.2047 13641	0.76
0.25	1.4674 62209	1.2110 56028	0.75
0.26	1.4630 85873	1.2173 20955	0.74
0.27	1.4586 88155	1.2235 11839	0.73
0.28	1.4542 68698	1.2296 31828	0.72
0.29	1.4498 27128	1.2356 83836	0.71
0.30	1.4453 63064	1.2416 70567	0.70
0.31	1.4408 76115	1.2475 94538	0.69
0.32	1.4363 65871	1.2534 58093	0.68
0.33	1.4318 31919	1.2592 63421	0.67
0.34	1.4272 73821	1.2650 12576	0.66
0.35	1.4226 91133	1.2707 07480	0.65
0.36	1.4180 83394	1.2763 49943	0.64
0.37	1.4134 50127	1.2819 41668	0.63
0.38	1.4087 90839	1.2874 84262	0.62
0.39	1.4041 05019	1.2929 79239	0.61
0.40	1.3993 92139	1.2984 28034	0.60
0.41	1.3946 51652	1.3038 32008	0.59
0.42	1.3898 82992	1.3091 92448	0.58
0.43	1.3850 85568	1.3145 10576	0.57
0.44	1.3802 58774	1.3197 87557	0.56
0.45	1.3754 01972	1.3250 24498	0.55
0.46	1.3705 14505	1.3302 22453	0.54
0.47	1.3655 95691	1.3353 82430	0.53
0.48	1.3606 44814	1.3405 05388	0.52
0.49	1.3556 61135	1.3455 92245	0.51
0.50	1.3506 43881	1.3506 43881	0.50
k_1^2	E	E	k^2

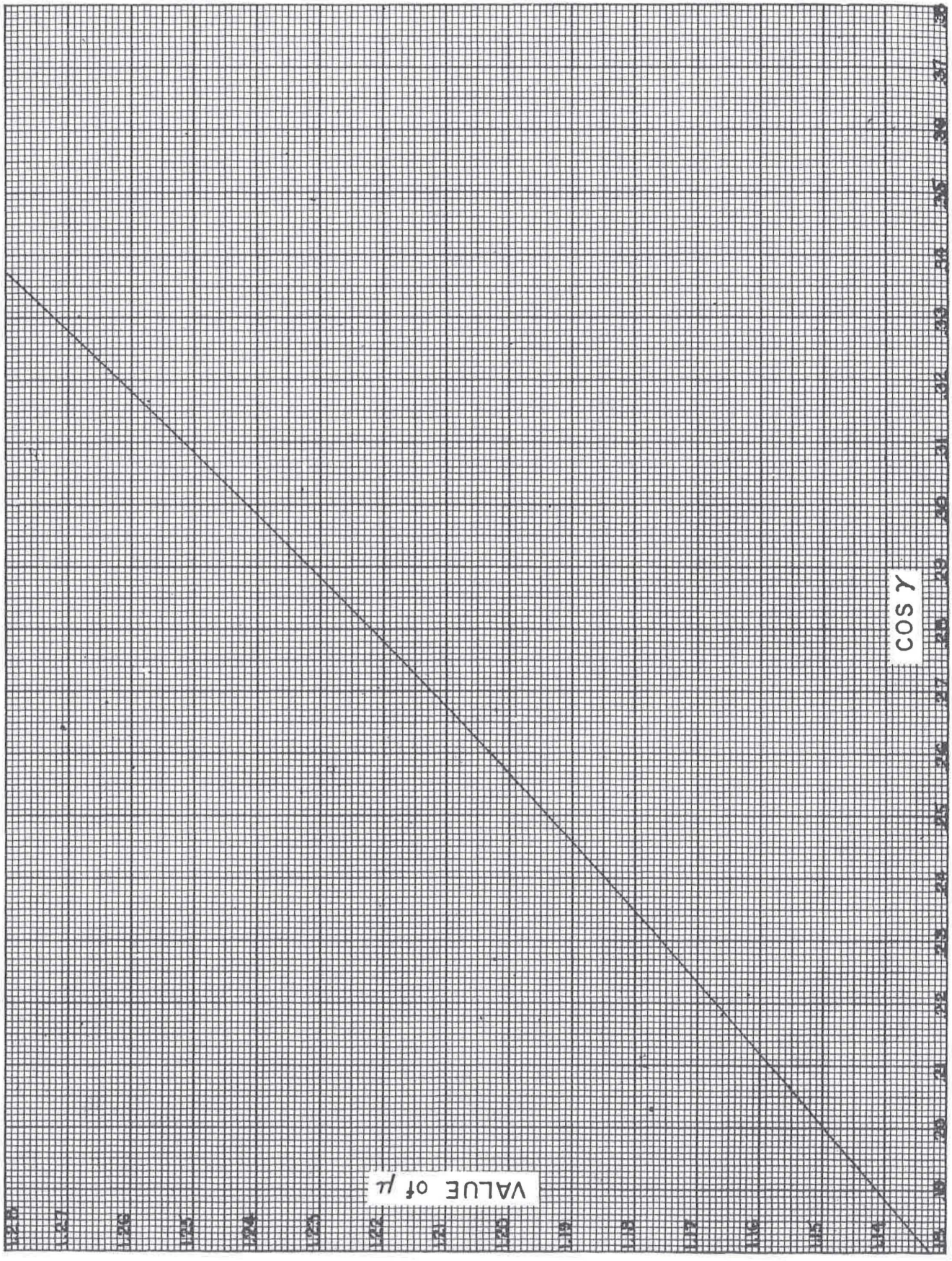
From: *Table Of The Complete Elliptic Integrals K, K′, E, E′,* by L. M. Milne-Thomson.

American Axle v. Neapco - IPR2025-00090
PET_AAM_1012-0356

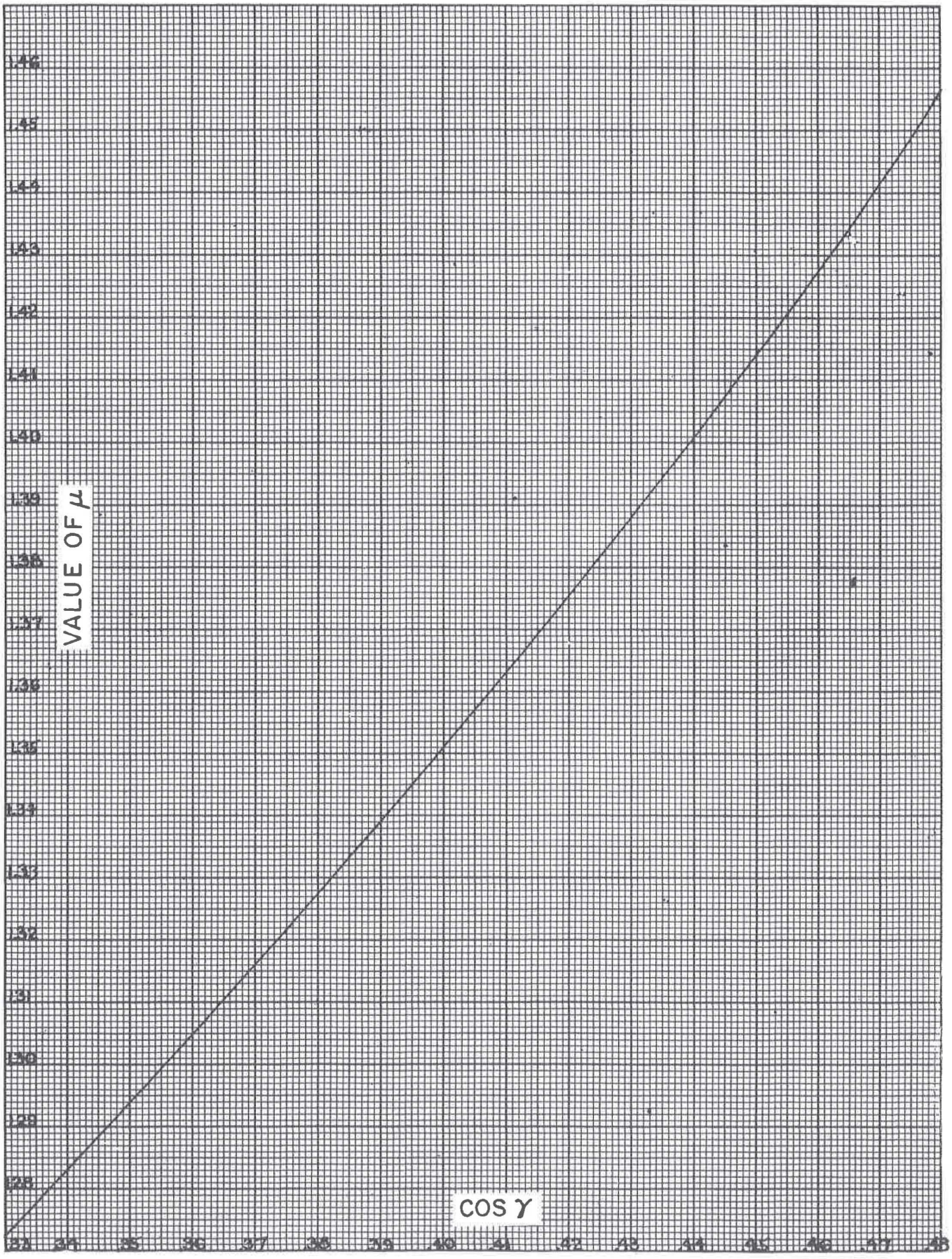


American Axle v. Neapco - IPR2025-00090
PET_AAM_1012-0357

Chart A-4

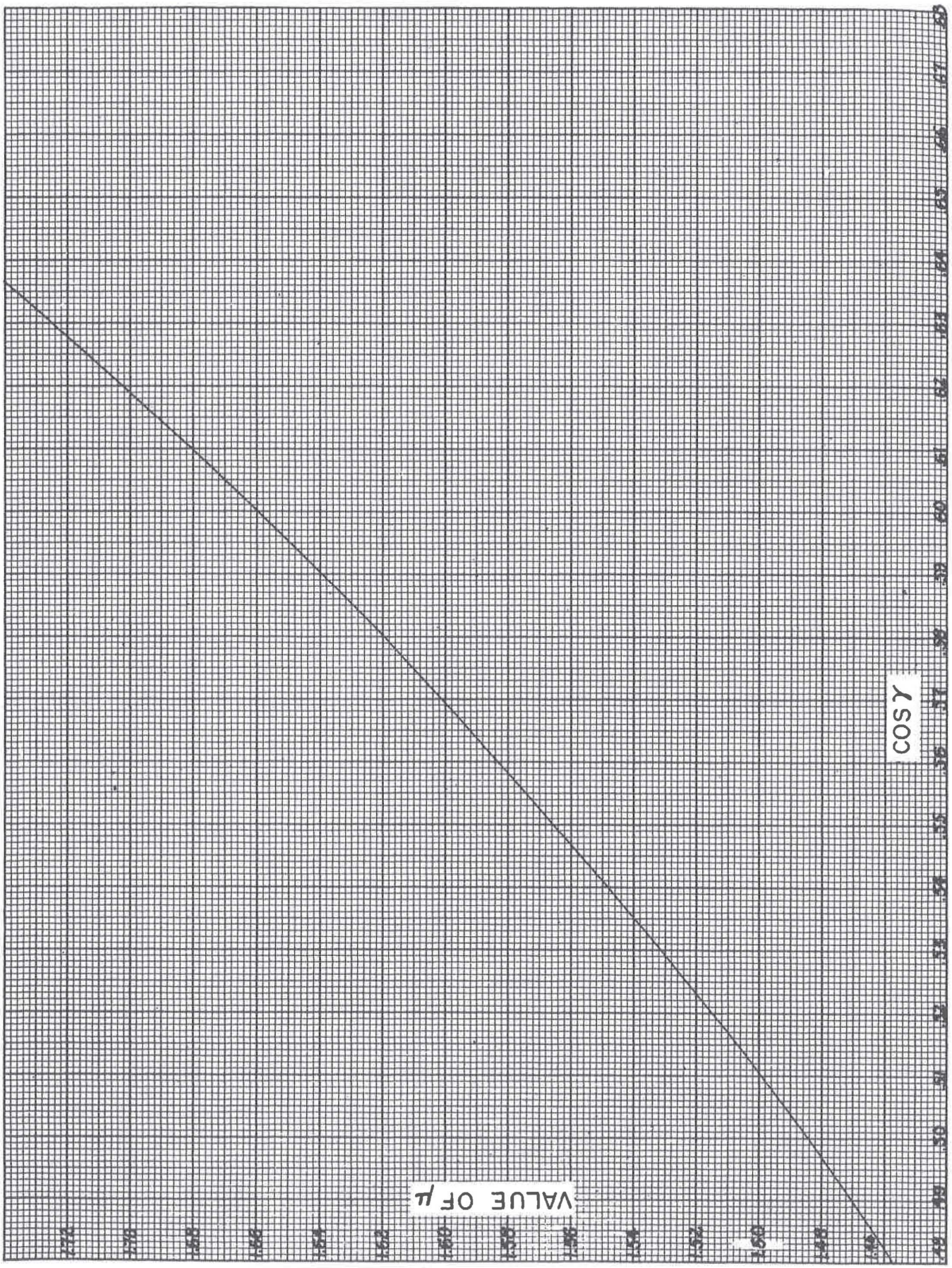


American Axle v. Neapco - IPR2025-00090
PET_AAM_1012-0358

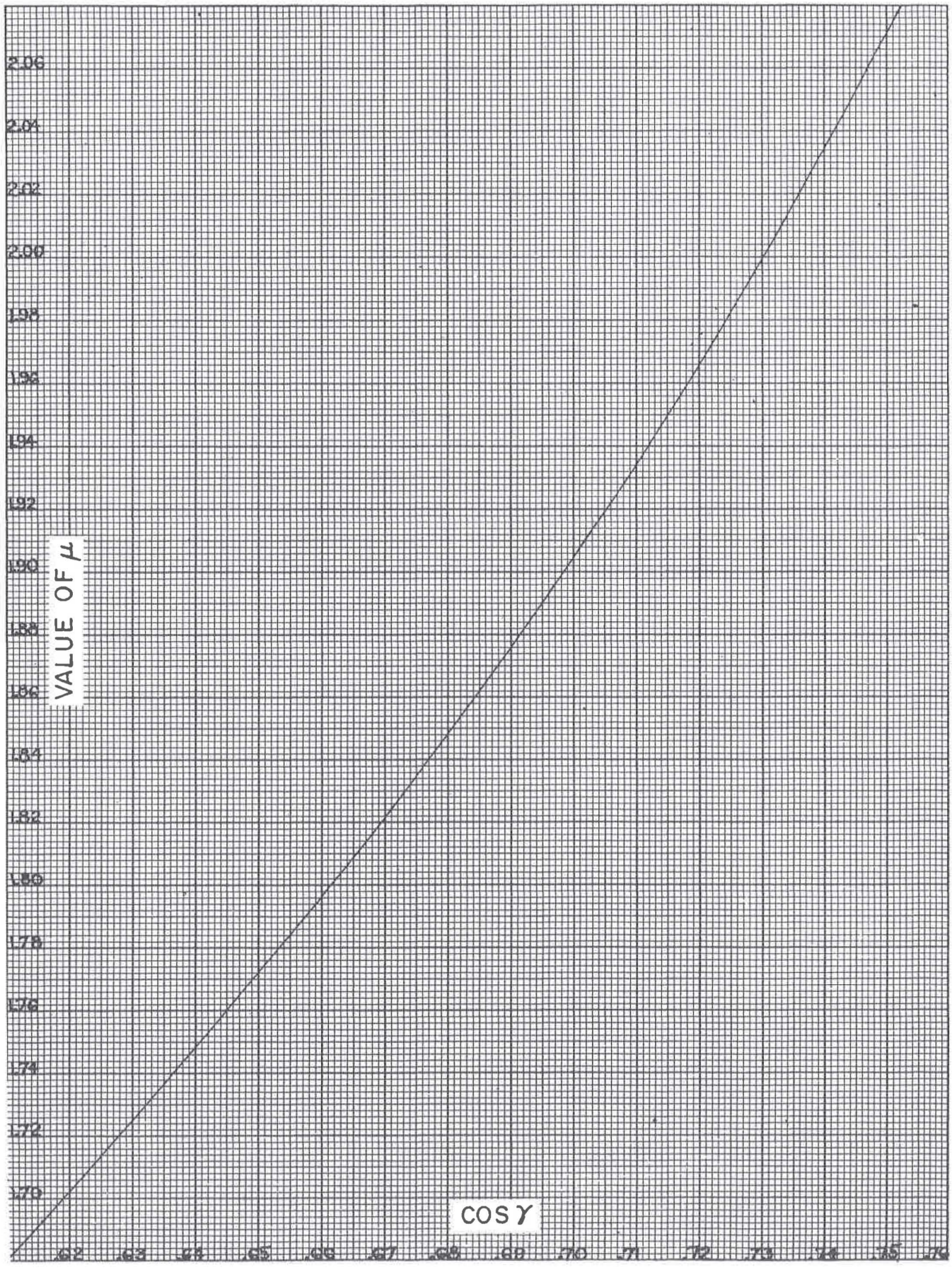


American Axle v. Neapco - IPR2025-00090
PET_AAM_1012-0359

Chart A-6

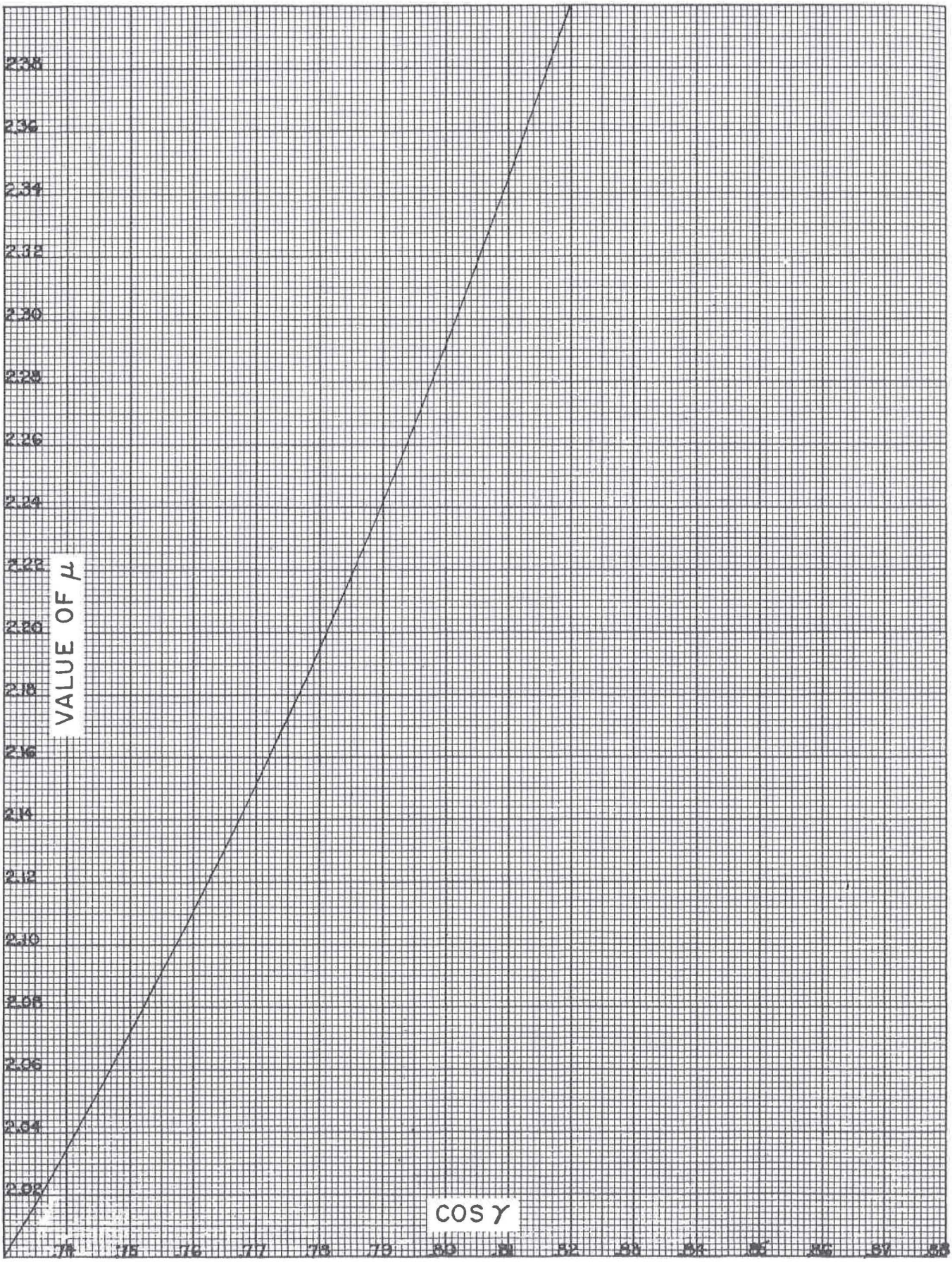


American Axle v. Neapco - IPR2025-00090
PET_AAM_1012-0360

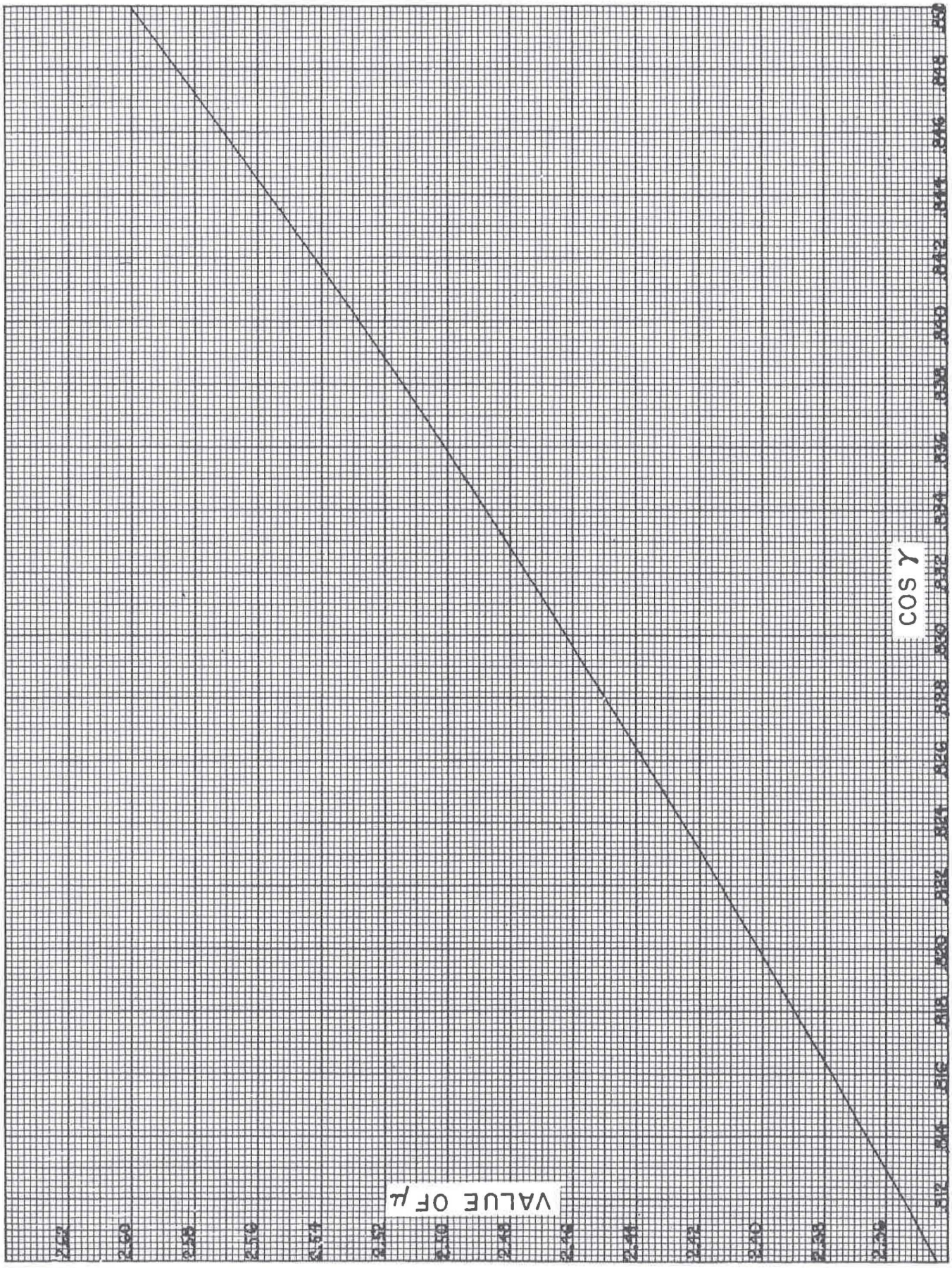


American Axle v. Neapco - IPR2025-00090
PET_AAM_1012-0361

Chart A-8

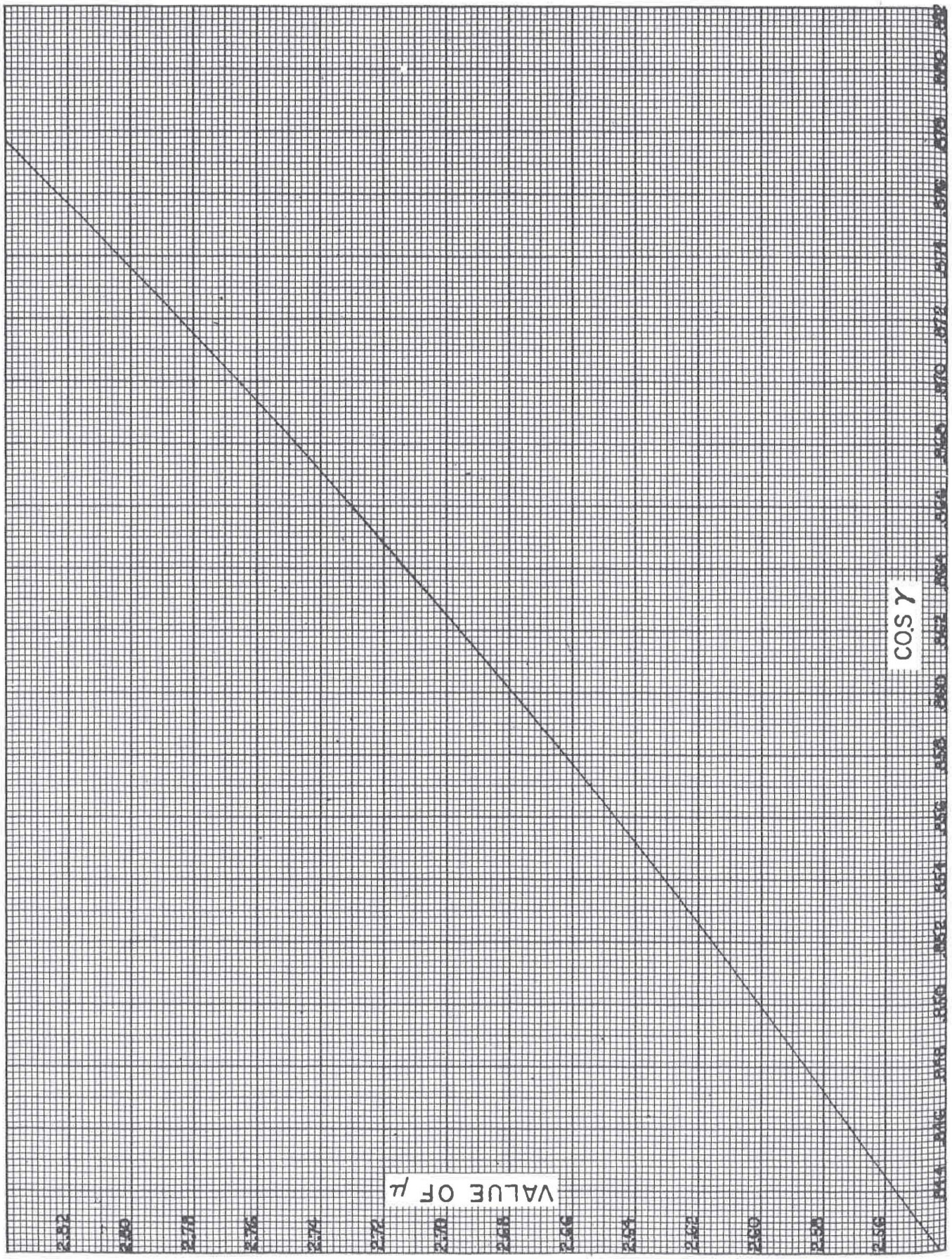


American Axle v. Neapco - IPR2025-00090
PET_AAM_1012-0362

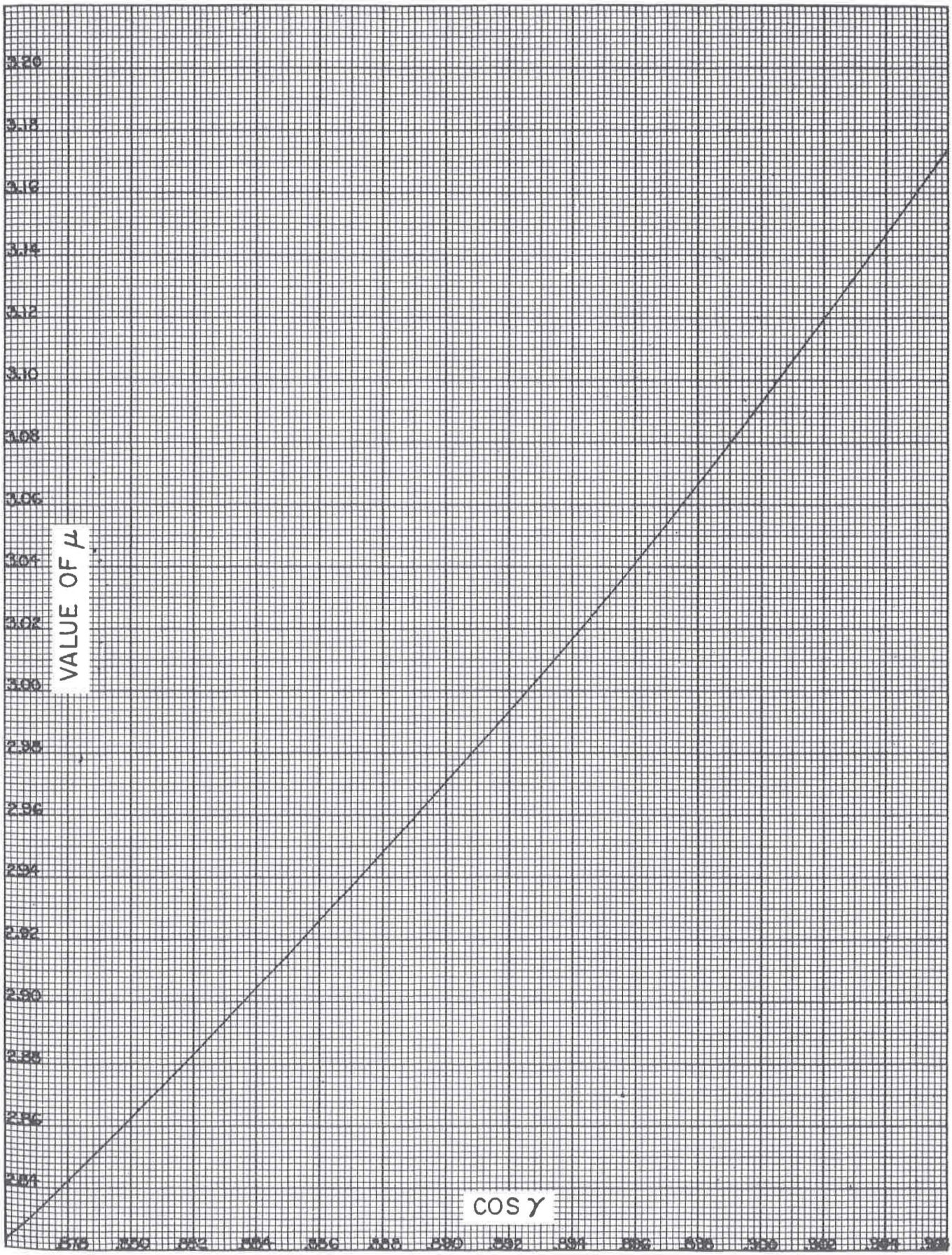


American Axle v. Neapco - IPR2025-00090
PET_AAM_1012-0363

Chart A-10

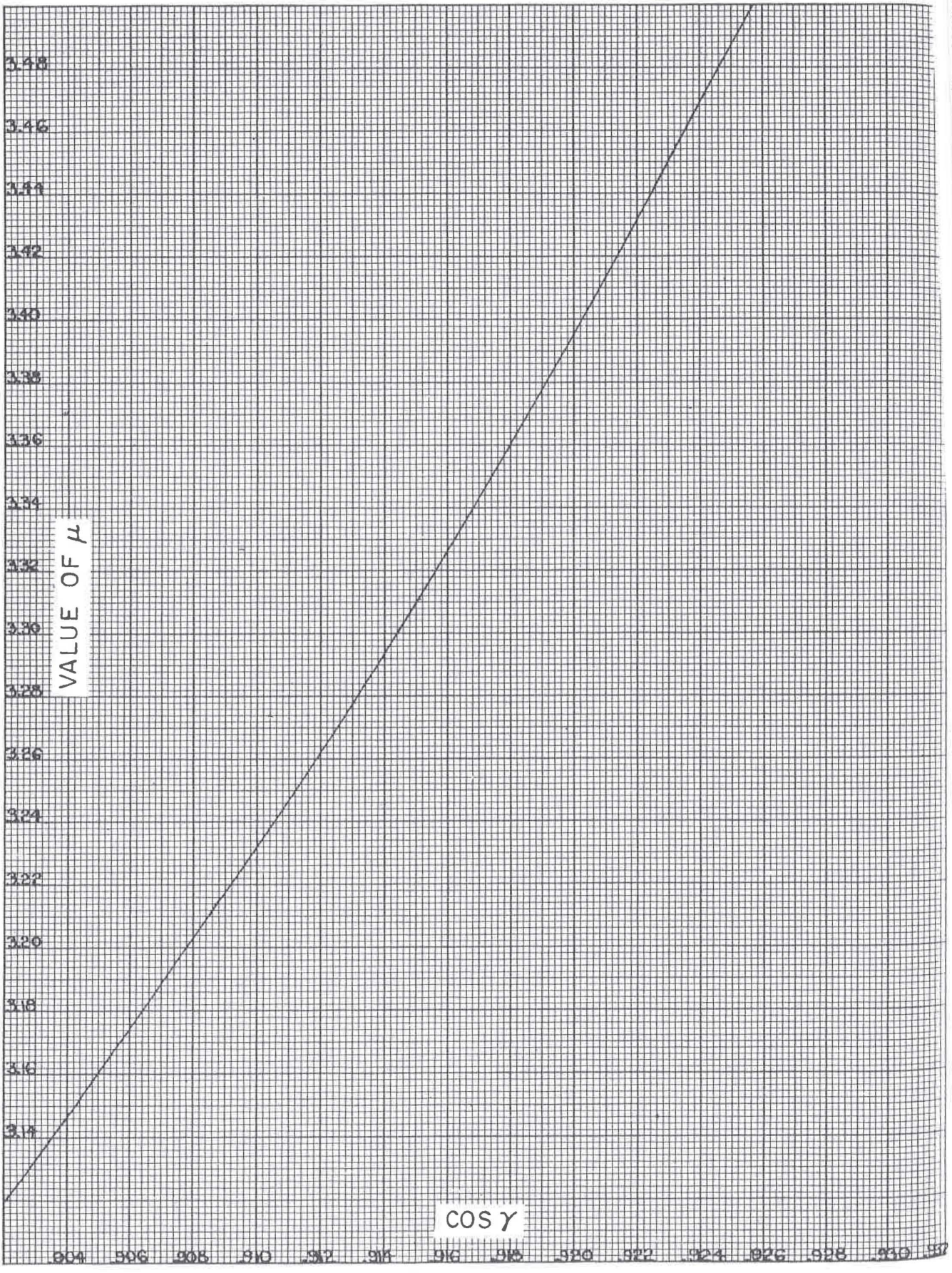


American Axle v. Neapco - IPR2025-00090
PET_AAM_1012-0364



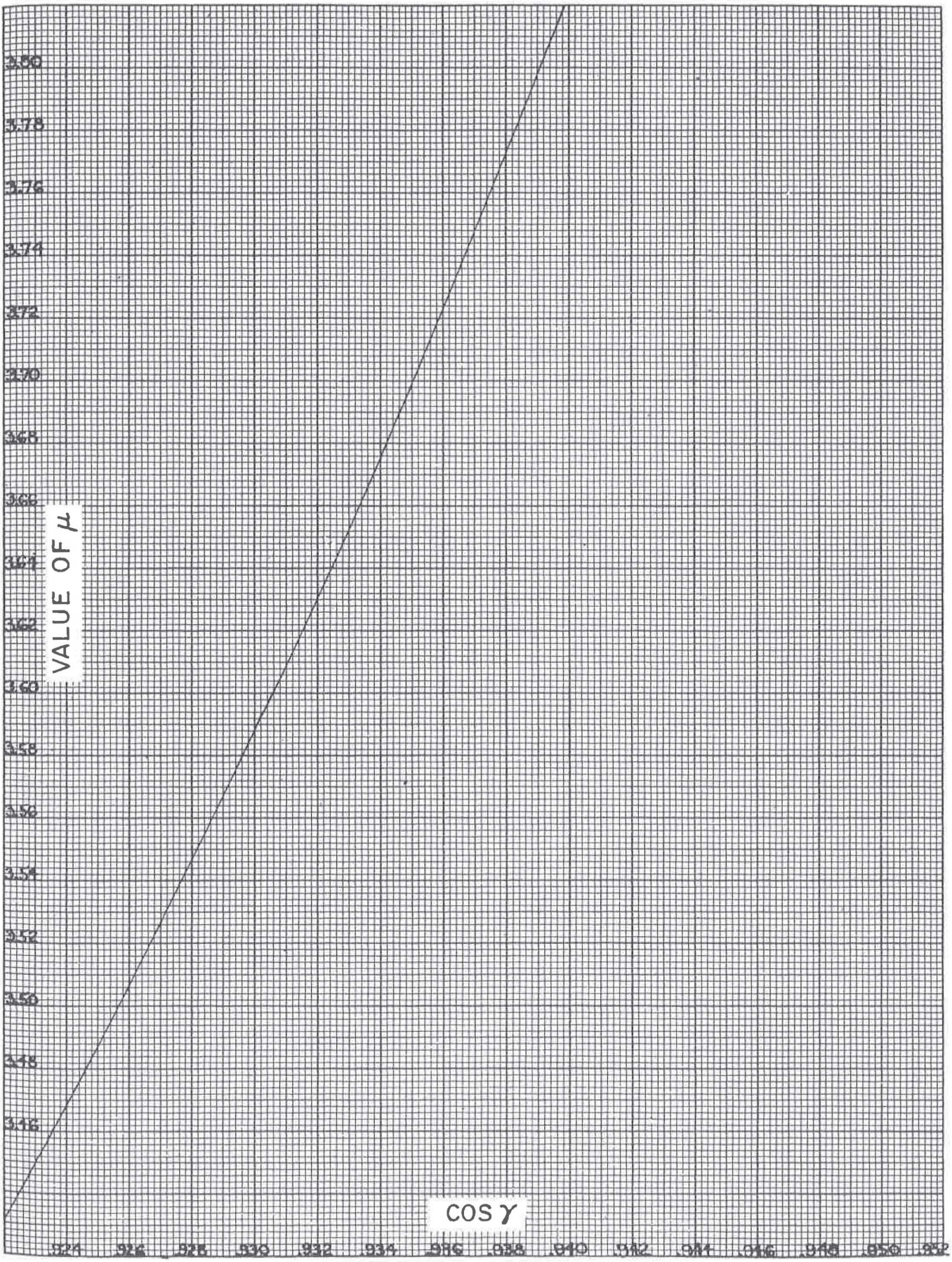
American Axle v. Neapco - IPR2025-00090
PET_AAM_1012-0365

Chart A-12



American Axle v. Neapco - IPR2025-00090
PET_AAM_1012-0366

Chart A-13



American Axle v. Neapco - IPR2025-00090
PET_AAM_1012-0367